Investigation of CRISPR-Cas9 as a novel method to generate organ-deficient mouse model for blastocyst complementation

Jonathan Jun-Yong Lim

Nara Institute of Science and Technology

Graduate School of Science and Technology

Division of Biological Science

Organ Developmental Engineering Laboratory

Associate Professor Ayako Isotani

Submitted on 1st August 2022

Division of Biological Science   Abstract of Doctoral Thesis

Laboratory (Supervisor)	Associate Professor Ayako Isotani			
Name	Jonathan Jun-Yong Lim		Date	June 29, 2022
Title	Investigation of CRISPR-Cas9 as a novel method to generate organ-deficient mouse model for blastocyst complementation			

The field of regenerative medicine aims to overcome organ shortage through methods like blastocyst complementation. This technique requires organ-deficient embryos to generate transplantable organs. By injecting pluripotent stem cells (PSCs) into organ-deficient embryos, organs can be generated solely of stem cell-origin, depending on the type of organ agenesis of the embryo.

The gene knockout model for blastocyst complementation provided methods to generate organ-deficient embryos. However, many genes are involved in the developmental processes of multiple organs and tissues, thus reducing the specificity to target a single organ of interest. Conditional cell ablation technique combining *Cre/loxP* technology and diphtheria toxin A (DTA) has also been frequently used to generate organ-deficient embryos. However, there are challenges such as toxicity from DTA affecting some other tissues and inducing unspecific cell death. Thus, this study investigates a novel CRISPR-Cas9-based strategy to generate organ-deficient mouse models by inducing cell death with single-guide RNA targeting at multiple sites (sgRNA^{ms}) in the genome.

First, doxycycline-induced *Cas9-EGFP* HEK293T cell lines were established for *in vitro* experiments to investigate the downstream effects of the Cas9-sgRNA^{ms} system. Upon Cas9 expression, an increase in γH2AX intensity was observed in the cell lines expressing sgRNA^{ms}. Furthermore, sgRNA^{ms}-expressing cell lines also showed an increase in the early and late apoptosis cell population, suggesting cell death was due to extensive DNA damage. These cell lines also showed a decrease in cell proliferation rate using the MTT assay and BrdU immunostaining. Additionally, the Cas9-sgRNA^{ms} system contributed to cell ablation in mouse ESCs. The knockout of *p53* in mESCs showed a decrease in apoptosis population upon expression of *Cas9-sgRNA^{ms}*. The evidence supports the hypothesis that the designed *Cas9-sgRNA^{ms}* system managed to induce cell death via the *p53* pathway *in vitro*.

Through the expression of Cas9 under an organ-specific promoter, coupled with constitutive expression of *sgRNA^{ms}*, cell death was hypothesized to occur in cells of the targeted organ. This study aimed to produce a thymus-deficient mouse model as a proof of concept. A mouse model was established with *Cas9* knocked in under the *Foxn1* promoter, and *hU6-sgRNA^{ms}* knocked in at the *Rosa26* locus, the feasibility of thymic epithelial cells ablation to produce a thymus-deficient mouse model was investigated in this study. *Foxn1^{Cas9};Rosa26_ms1* and *Foxn1^{Cas9};Rosa26_ms2* mice were evaluated for the ablation of the thymus. These progenies showed an athymic phenotype, similar to the nude mouse, and CD3$^+$/CD45$^+$ T cells were not detected in the peripheral circulatory system, confirming the lack of a functional thymus in these mice. Blastocyst complementation of *Foxn1^{Cas9};Rosa26_ms* embryos with rat ESCs showed the successful generation of rat cells-derived thymus in mouse embryos.

This study provides a novel technique to generate organ-deficient embryos by CRISPR-Cas9-based method, using multiple-site targeting sgRNA.

Table of contents

Chapter 1 – Introduction

1.1   Fundamental research in regenerative medicine

Organ failure is one of the main issues affecting overall human health and lifespan, caused by disease and aging. The main treatment plan for irreversible organ failure is solid organ transplantation. Although organ transplantation technology has improved over the past decades, the supply and demand gap for transplantable organs is still very wide at the global level (Figure 1). Thus, to overcome the problem of organ shortage, the field of regenerative medicine has come up with the idea of growing transplantable human organs in the body of other animal species.

Organ shortage problem
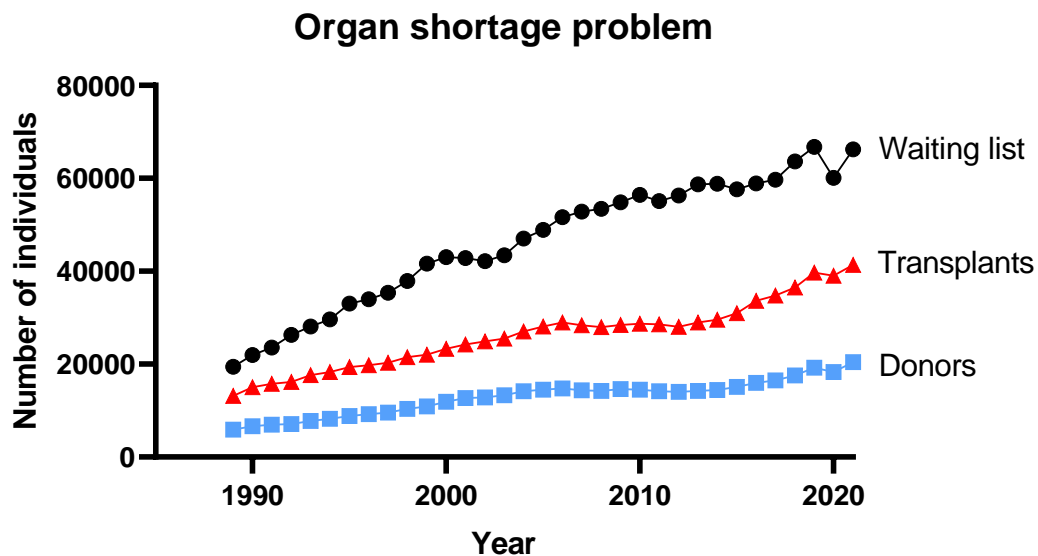
From UNOS database, 2022

Figure 1: Comparison of the number of patients on the waiting list, number of organs donors, and number of transplants performed

One of the methods to overcome organ shortage is to increase the number of organs available for transplantation. Living donors can donate part of the liver or one of the kidneys to a patient that is immunologically matched. However, organs such as the heart can only be obtained from patients that have been certified brain dead, a common criterion across Japan and many countries[1]. It was reported that the incidence of brain death is extremely low, at about 2% in the United States, therefore contributing to the low number of available human donors[2]. Therefore, if we can obtain a large number of transplantable human organs from animals, then it could be possible to overcome the problem of organ shortage.

Xenotransplantation is the procedure of transplanting cells, tissues, or organs originating from one species to another species. This has been one of the promising ideas since it allows growing organs needed for human transplantation in other animal species, in large quantities. However, immunological rejection of interspecies organ transplantation is the main

hurdle in xenotransplantation. To produce human organs through interspecies chimeric animals, certain genetic modifications must be made to the host animal.

Pluripotent stem cells (PSCs) such as embryonic stem cells (ESCs) were found to have pluripotency to differentiate into all tissue types of the originating organism. These ESCs can be harvested from preimplantation embryos and cultured under controlled conditions[3,4]. Furthermore, the generation of human induced pluripotent stem cells (iPSCs) from somatic cells has also been reported[5], thus overcoming the ethical dilemma of generating human stem cells from embryos. Immunological rejection can also be overcome with iPSC-derived cells in autologous transplantations[6]. Current experimental tools such as stem cells and chimeric animals play a major role in elucidating organ development processes, in both intra- and interspecies chimeras. This forms the basis for the idea of generating transplantable human organs from laboratory animals.

Through the blastocyst complementation technique, PSCs can be injected into an organ-deficient blastocyst to obtain a chimeric animal. The injected stem cells then fill up the niche of certain missing organs or cell types of the host blastocyst, hence, generating organs or cell types fully derived from the stem cells (Figure 2). This technique has been reported to be successful in generating different organs in intra- and interspecies chimera[7–10]. However, this presents a major problem. Host animals lacking a certain organ are usually lethal at the prenatal stage and cannot produce blastocyst for complementation. Since it is impossible to maintain organ-deficient animals to obtain their blastocyst, these blastocysts are usually produced by interbreeding between two animals with heterozygous knockout (KO) of organ-specific genes[9,11], resulting in using a high number of mice. Therefore, this study aims to develop a novel approach using CRISPR-Cas9 mediated cell ablation to generate an organ-deficient mouse model and blastocyst.
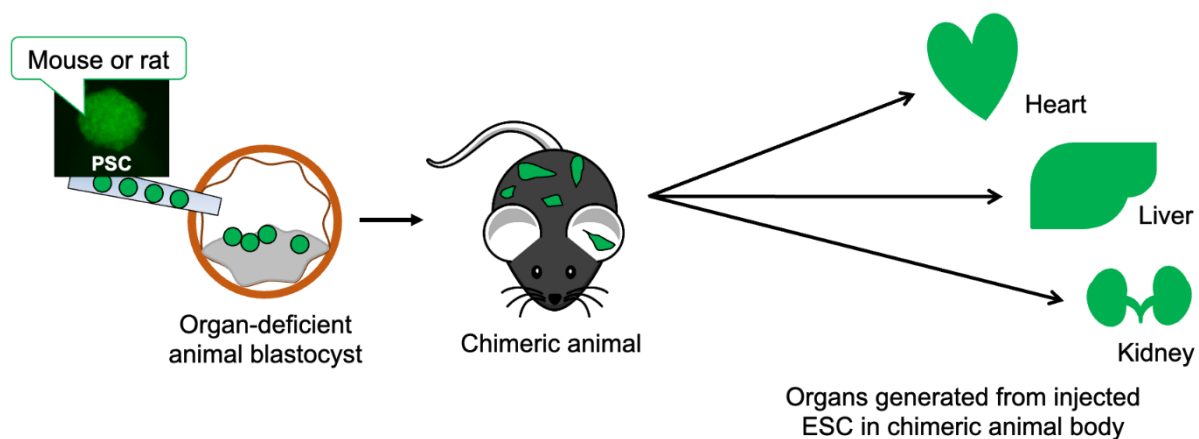

Figure 2. Schematic diagram of the blastocyst complementation method to generate organs using chimeric animal models

1.2   Generation of organ-deficient animals

The conventional gene KO technique has been used to obtain organ-deficient mouse models. This technique requires the introduction of a targeting vector into ESCs. This vector of foreign DNA consists of an antibiotic resistance gene for positive selection, flanked with homologous arms at the upstream and downstream regions. The antibiotic resistance gene integrates into the target gene through a homologous recombination mechanism, disrupting normal genetic sequence and KO target genes. In addition, the antibiotic resistance gene acts as a positive selection marker to help researchers correctly identify ESC clones with targeted gene KO (Figure 3). After obtaining KO cell lines, they are then injected into mouse blastocyst to obtain chimeric mice. By mating this chimera, the next generation mice can be obtained for further breeding to generate homozygous KO mouse models[12].

Mouse PSCs can be injected into gene KO blastocyst with organ agenesis to obtain the organs of interest. Generally, organ-deficient animal models with homozygous gene KO are not viable. Therefore, we need to maintain the heterozygous mutant. However, the probability to obtain a homozygous KO embryo is only one-fourth of all embryos by crossing heterozygous parents. This system is not the best in terms of cost, labor efficiency, and animal welfare.

Furthermore, in certain gene KO models, injected PSCs can rescue and maintain the survival of host cells with gene KO, resulting in organs with a mix of host and PSC-derived cells[13]. The gene KO method cannot be used on genes involved in developmental pathways of multiple organs to generate specific organ-deficiency models, because the development of many other organs is also disrupted.
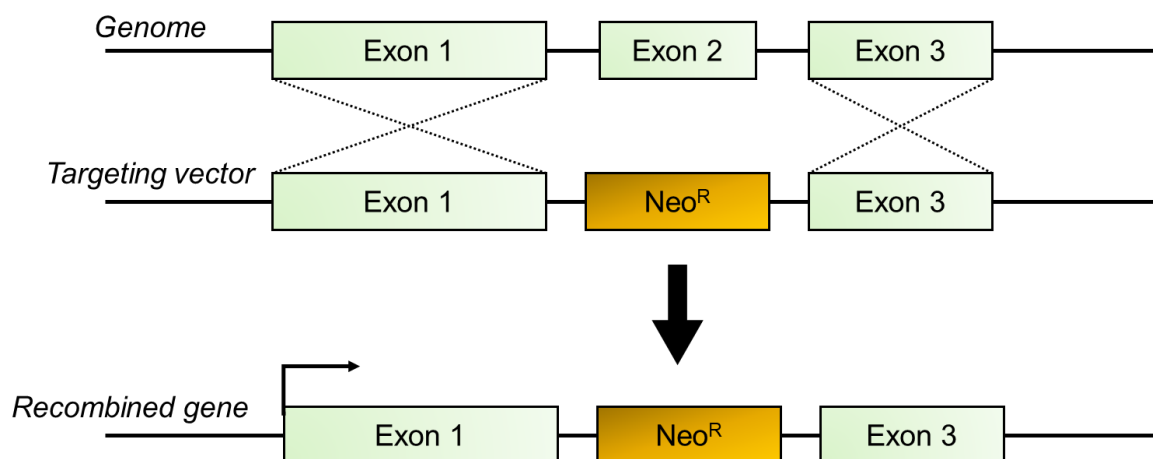
Figure 3. Conventional gene KO method through homologous recombination

Another method to generate lineage-specific ablation animal models is by using diphtheria toxin A (DTA) to induce cell death[14]. Since its discovery, it has been widely used for targeted cell ablation applications such as targeting pancreatic cells[14], germ cells[15], and photoreceptor cells[16]. Cells expressing this protein of high toxicity undergo cell death due to inhibition of protein synthesis[17–19]. It has been reported that even one molecule of this toxin is enough to kill the cell[20]. Since most organ development processes are pleiotropic and polygenic,

thus it is necessary to restrict the expression of DTA and limit its effect through other control systems.

Cre/LoxP system has been well established in the field of animal genetics for the spatial and temporal control of gene expression[21]. This system consists of a site-specific *Cre* recombinase protein controlled by a tissue-specific promoter, and a *LoxP* site, a 34-base pair (bp) DNA sequence, that is recognized by *Cre* recombinase. The gene of interest is flanked by *LoxP* sites, and upon expression of *Cre* recombinase, the gene sequence between the two *LoxP* sites in the same direction is excised, causing gene KO in a tissue-specific manner. The *Cre/LoxP* system is useful to perform conditional cell KO[8,9].

The conditional cell ablation method uses *Cre/LoxP* system to induce the expression of DTA protein by generating a transcriptional termination element (STOP) flanked by two *LoxP* sites, located upstream of the DTA cassette. In tissues with an active expression of *Cre* recombinase, the *LoxP* sites are excised and the downstream DTA gene is expressed, leading to tissue-specific cell death (Figure 4). This conditional cell ablation method has been widely used to generate tissue- and organ-deficient mouse models[15,22,23].

Several limitations of such conditional ablation systems have been reported. Administration of diphtheria toxin was found to cause local inflammation even in wild-type control mice[24], and results from such applications must be thoroughly examined. This phenomenon could not exclude the possibility of the toxicity effects of DTA on lymphocytes that engulf apoptotic cells. Furthermore, the *Cre*-mediated excision of *LoxP* sites was not 100% efficient across all *Cre*-expressing cells and produced mosaic phenotype[25]. If the progenitor stem cells were not completely ablated, there is a possibility that the tissue or organs could be generated.
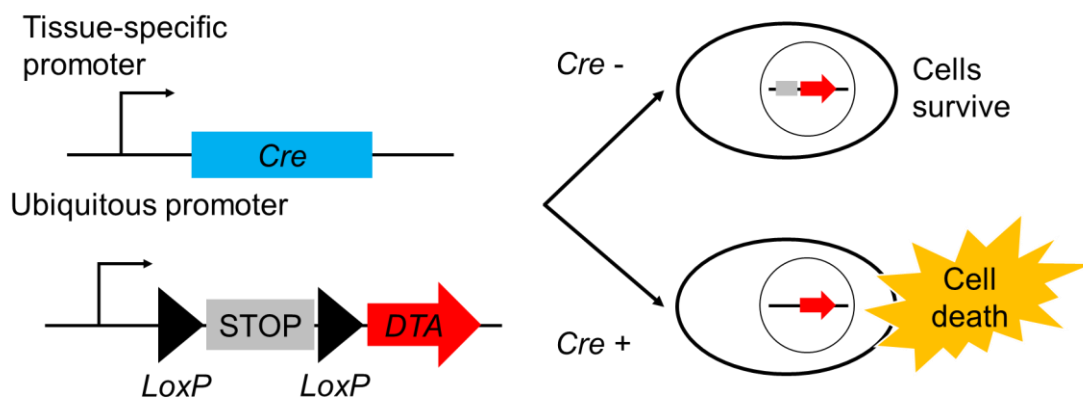
Figure 4. Schematic diagram of *Cre-LoxP* conditional cell ablation mechanism

1.3 CRISPR-based genome editing systems

The clustered regularly interspaced short palindromic repeats (CRISPR) and CRISPR-associated (Cas) protein were initially discovered in bacterial immunity to fight against virus[26]. The bacterial immune system includes three different steps, namely (1): adaptation; (2): expression; and (3): interference stage[27]. When a virus invades a bacterium, the viral DNA is

injected into the host and bacteria use the CRISPR system during the adaptation stage to recognize and acquire short viral DNA fragments. This viral DNA sequence, known as the protospacer sequence, is then integrated into the CRISPR locus. When a new virus invades a bacterium, a new protospacer sequence then integrates into the CRISPR locus, rendering the bacteria to be immunized against this new virus. In the expression stage, the CRISPR locus is transcribed to produce a precursor CRISPR RNA (pre-crRNA), which then matures into crRNA by Cas proteins. During the interference stage, crRNA forms a complex with Cas proteins and guides Cas proteins to target and cleave DNA from invading viruses[28,29].

CRISPR-Cas system has been classified into two major classes and five types, depending on the effector Cas proteins involved in the interference stage and crRNA maturation pathways. Each different classes and types possess unique composition in the expression, interference, and adaptation stages. The class 1 CRISPR-Cas system is further divided into type I, type III, and type IV systems, whereby multiple Cas proteins are required to carry out the cleavage of target DNA. In the class 2 CRISPR-Cas system, both type II and type V require only one single protein to carry out DNA cleavage, thus revolutionizing the field of genome editing due to its simple production and manipulation of the Cas protein and crRNA[30]. Furthermore, another component known as a protospacer adjacent motif (PAM), a short, conserved sequence that is present downstream of the non-complementary strand in target DNA, is required to allow Cas9 binding before DNA cleavage.

1.3.1 CRISPR-Cas9 system

A widely known CRISPR-based protein that was used in the field of genome editing is the CRISPR-Cas9 system, which is a type II CRISPR-Cas system (Figure 5). For Cas9 to carry out its function, two types of RNA are required, namely crRNA and trans-activating crRNA (tracrRNA). The crRNA guides Cas9 protein to target sites while tracrRNA acts as a bridge to link crRNA and Cas9, forming a protein-RNA complex. To further simplify its application, a group of researchers cleverly linked the two RNA components into one, known as single-guide RNA (sgRNA)[28]. The PAM sequence of Cas9 is 5'-NGG-3'. By designing and manipulating the sgRNA sequence, Cas9 protein can induce double-strand break (DSB) at virtually any sites complementary to the sgRNA due to the abundance of the PAM sequence. The presence of DSB facilitates gene KO by inducing insertion and deletion (indel) mutation through DNA repair mechanisms, and gene knock-in through homologous recombination with targeting vectors. Further research by other groups appended nuclear localization signal (NLS) upstream and downstream of Cas9, to direct Cas9 into the nucleus of mammalian cells and to carry out gene editing[31,32].

Researchers have conducted many genome editing experiments, especially by knocking-out organ-specific genes using Cas9 and customized sgRNA, resulting in organ-deficiency[9,33,34]. The lack of these important organ-determining genes and proteins led to organ agenesis due to the disruption in key developmental pathways[35]. However, most of the organ

developmental processes involve multiple pleiotropic genes and generating organ-specific deficient animal models is not feasible through the gene KO method because many other tissues could potentially be affected, rendering the animal inviable.

1.3.2   CRISPR-Cpf1 (Cas12a) system

In the type V CRISPR-Cas system, a lesser-known protein of Cpf1 (also known as Cas12a) recently gained more attention in the field of genome editing[27,36–38]. This is because it has major differences compared to Cas9 protein (Figure 5). Instead of only cleaving target DNA like Cas9, Cpf1 can cleave both DNA and RNA target sequences. Moreover, the PAM sequence recognized by Cpf1 is 5'-TTTV-3', which is located upstream of the protospacer sequence. This is useful when researchers intend to conduct genome editing in A-T-rich regions[37]. Another difference is that the cleavage induced by Cpf1 is a staggered cut with 5 – 8 nucleotides overhang[36], like a sticky end produced by restriction enzyme, compared to a blunt end DSB cut produced by Cas9. Furthermore, only the crRNA is required for the Cpf1 function, which is shorter than the sgRNA for Cas9.
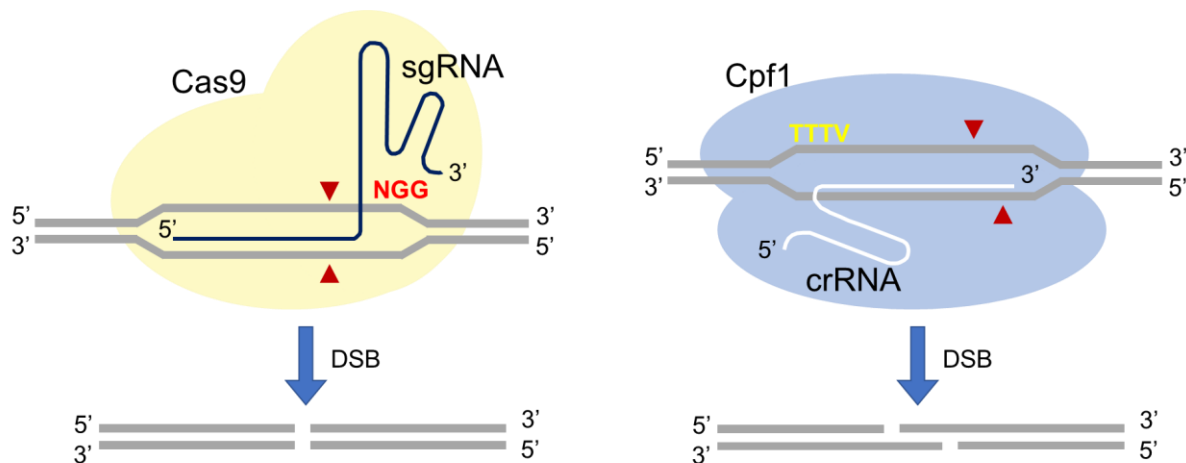
Figure 5. Schematic diagram comparing between CRISPR-Cas9 and CRISPR-Cpf1

1.4   CRISPR-Cas9 mediated cell ablation

CRISPR-Cas9 has also been frequently employed in the field of cancer therapy. By introducing multiple-sites DNA DSB in the genome of cancer cell lines[39,40] or targeting cancer-specific fusion oncogenes[41], cell death was induced in several cancer cell lines. Furthermore, CRISPR-Cas9 has also been employed to knockout anti-apoptosis genes in tumors[42,43]. Taken together, these studies suggested that by introducing multiple-site DNA DSB, the extensive DNA lesion was able to trigger apoptosis in a cell type-specific manner. Thus far, there have yet to be trials on introducing DNA DSB in an organ-specific manner to generate an organ-deficient mouse model for blastocyst complementation.

11

This study aims to test a new method to generate organ-deficient mouse models using the CRISPR-Cas9 system in an organ-specific fashion and using sgRNA that targets multiple sites (sgRNA^{ms}) in mouse genomes. The designed Cas9-sgRNA^{ms} system is hypothesized to induce genome-wide DNA DSB in organ-specific cell lineage, induce cell ablation, and eventually generate an organ-deficient mouse model (Figure 6). By changing the promoter that controls Cas9 expression, this system could potentially be used to generate mouse models of different organ-deficiency.
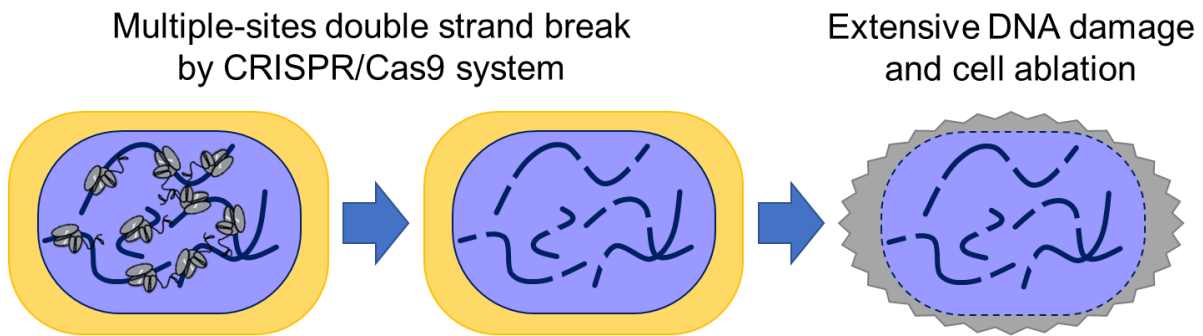
Figure 6. Schematic diagram showing mechanism of multiple-site DNA DSB by Cas9-sgRNA^{ms} system, leading to cell ablation and to generate organ-deficient model.

1.5   DNA damage response

Apart from the method using DTA to induce apoptosis, DNA damage and lesions that were left unrepaired can also lead to cell death. DNA damage caused by ultraviolet (UV)-induced damage and alkylating agents can lead to DNA mismatch and inter-strand DNA crosslinking, and eventually cell death[44]. DNA damage triggers downstream DNA damage response (DDR) as a fast and complex response to activate a cascade of proteins for cell survival maintenance. DNA DSBs and stalled DNA replication forks trigger DNA damage sensors such as ataxia telangiectasia-mutated (ATM), and ataxia telangiectasia and Rad3-related (ATR). In addition, DNA-dependent protein kinase catalytic subunit (DNA-PKcs) were also recruited to DSB sites[45,46]. This ATM/ATR/DNA-PKcs kinase pathway is the start of DDR that initiates DSB repair, cell cycle checkpoints activation, and triggers apoptosis cascade[44] (Figure 7).

At DNA DSB sites, the activation of the DDR pathway first initiates phosphorylation of histone H2AX at serine 129 (γH2AX)[47,48]. The recruitment of the MRN complex (MRE11-RAD50-NBS1) at DSB sites creates a positive feedback loop by further activating ATM, causing the spread of H2AX phosphorylation. This leads to the formation of γH2AX foci at DSB sites and has long been used as a biomarker to detect DNA DSB[49]. It has been reported that the number and intensity of γH2AX foci increase with the amount of DSB present in cells[50].

DNA repair occurs in cells via two major pathways, non-homologous end joining (NHEJ), and homology-directed repair (HDR), depending on the cell cycle phase[51]. Generally, the NHEJ pathway is more predominant than HDR and is more error-prone because NHEJ

simply ligates two broken DNA ends without ensuring correct sequence information. Alternatively, HDR occurs predominantly in S and G2 phases. The broken strand of DNA utilizes the sister chromatid that is in close proximity as the template for repair[52]. DNA-PKcs are mainly involved in NHEJ through DNA-free end protection with the help of Ku70/80 heterodimer ring protein[53], while ATM involves in HDR via MRN complex[46].

Another protein involved in DDR is the tumor suppressor protein, p53, a gene product of *TP53*. In unstressed conditions, MDM2-bound p53 is subjected to proteasomal degradation. However, in the presence of DNA lesions and ATM/ATR activation, inhibition of MDM2 stabilizes p53, which causes p53 accumulation in cells[54]. P53 plays a central role in DDR as it is involved in both cell cycle arrest and apoptosis induction. In mammalian cells, p53 activates cell-cycle arrest through transcriptional activation of p21. P21 protein induces G_1 arrest through binding to cyclin E/Cdk2 and cyclin D/Cdk4 complexes[55]. Furthermore, p21 can block G_2/M transition through inhibition of cyclin B/Cdc2[56]. This allows cells to have time to repair DNA lesions before resuming the cell cycle.

Apart from cell cycle arrest, p53 is also involved in the induction of apoptosis via pro-apoptotic genes, such as BID, NOXA, and PUMA[54]. Simultaneously, p53 can also directly or indirectly inhibit anti-apoptotic genes such as *Bcl2* and *Mcl1*[57,58]. With the accumulation of p53 in the cytoplasm and activation of pro-apoptotic genes, these further cause mitochondrial outer membrane permeabilization (MOMP) to trigger apoptosis execution factors[59,60]. Cytochrome C leaks from mitochondria into the cytoplasm and forms apoptosomes with Apaf-1 to activate caspase-9, leading to apoptosis commitment[58]. Since p53 is the central protein in the network, it has been reported that the threshold between cell cycle arrest and apoptosis[58], and between pro- and anti-apoptosis genes[61], determines the activation of the apoptosis cascade. By inhibiting Bcl2-family genes, cells were found to be more sensitive toward p53-induced apoptosis[61].
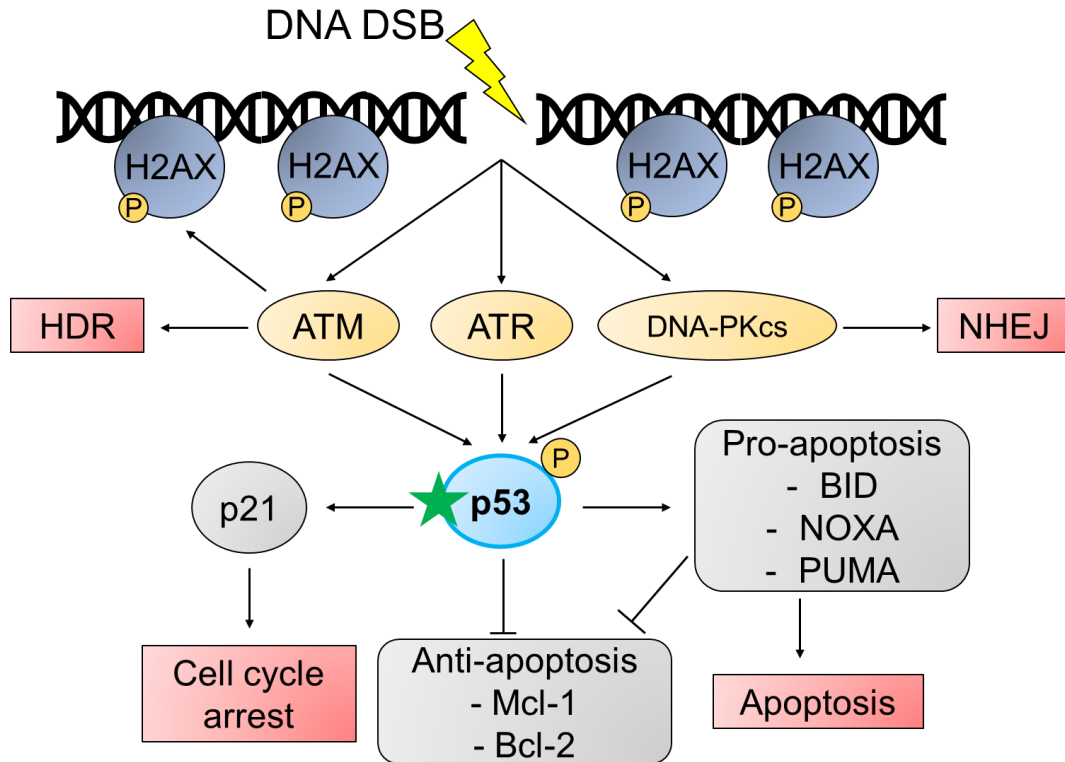
Figure 7. DNA damage response network in relation to cell cycle arrest and apoptosis

1.6   Thymus formation and its function

The thymus is a major organ in the adaptive immune system and acts as the site for T cell education, maturation, and differentiation. It also plays a major role in solid graft rejection[62]. The thymus is made up of two histologically distinct compartments, known as the cortex and the medulla, with functionally distinct cells, known as cortical thymic epithelial cells (cTEC) and medullary thymic epithelial cells (mTEC) (Figure 8). The cortex and the medulla meet at the corticomedullary junction (CMJ). Positive and negative selection of thymocytes occurs at the cortex and the medulla, respectively[63]. This thymic architecture is important for the T cell maturation process.
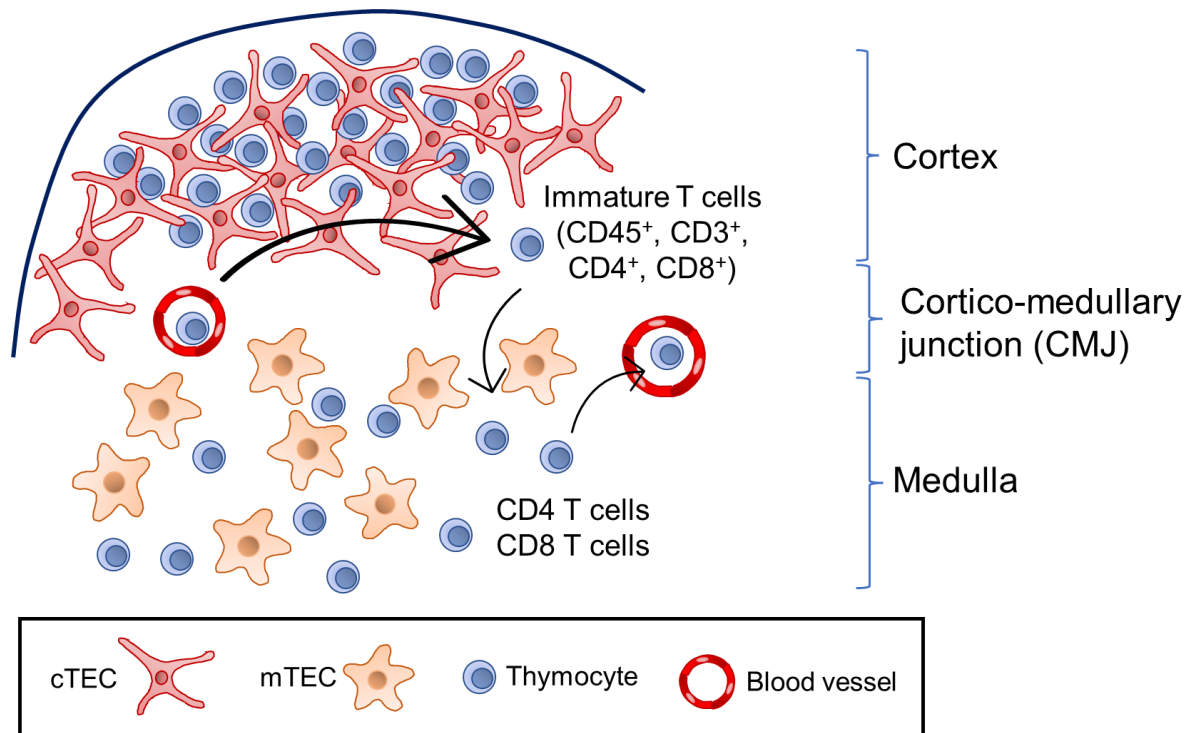
Figure 8. Schematic diagram of the thymus cross-section with different regions and cell populations

Thymus organogenesis was well-studied and found to be mainly controlled by the *Foxn1* gene which regulates the expression of the FOXN1 transcription factor. This expression is required for the differentiation of TECs, one of the major cellular communities in the thymus[63], apart from thymocytes. FOXN1 was found to be expressed as early as embryonic day 11.5 (E11.5), at the third pharyngeal pouch in mouse embryos[64,65]. Although FOXN1 expression was reported to sustain throughout the lifetime, FOXN1 expression level decreases from adulthood and leads to thymus involution[66–68].

The development of thymocytes and TECs are interdependent, through a process known as thymic crosstalk. This process is important for normal thymus development and maintenance of the integrity of the thymic microenvironment[69]. During development, early thymic progenitors (ETPs) migrate from bone marrow to thymus via chemotaxis[70,71]. These ETPs are $CD4^-CD8^-$ double negative and undergo T cell receptor (TCR) rearrangement after lineage commitment. Subsequently, CD4 and CD8 are expressed, developing into immature $CD4^+CD8^+$ double positive cells. In the thymus, they first encounter and interact with cTECs for positive selection by recognizing the major histocompatibility complex (MHC) on cTECs. Depending on their affinity to MHC class I or II, they then develop into $CD8^+$ and $CD4^+$ single positive T cells respectively[72]. Next, these cells migrate to the medulla to interact with mTECs for negative selection. mTECs present tissue-restricted antigens (TRA) on MHC molecules, which are controlled by *Aire* and *Fezf2*[73,74]. Developing T cells that interact strongly at this stage undergo apoptosis to prevent self-recognition and autoimmune syndrome[71]. The mature single positive T cells then migrate into the circulatory system.

Foxn1^{-/-} mouse was found to be athymic and have T cell deficiency and was termed as a *nude mouse* due to the lack of hair[75]. It was later mapped that this phenomenon was caused by a single base pair deletion in exon 3, causing a frameshift mutation and subsequently lacking the DNA-binding domain in the resultant FOXN1 protein[76]. Although most of the organ-deficient mouse models are non-viable, the lack of thymus and hair in *Foxn1*^{-/-} mouse does not affect the survivability and reproduction of this mouse. Therefore, this study targets to induce cell lineage ablation of the thymus using the CRISPR-Cas9 system.

1.7   Objective

As a proof of concept, the thymus was chosen as the target organ to test the method of generating an organ-deficient mouse model using CRISPR-Cas9 and sgRNA[ms] (Cas9-sgRNA[ms] system). It was hypothesized that Cas9-sgRNA[ms] cleave genomic DNA at multiple sites causing extensive DNA damage and inducing cellular defects. This research aims to investigate the effects of Cas9-sgRNA[ms] *in vitro* using HEK293T and mESCs, and to produce a thymus-deficient mouse model using the Cas9-sgRNA[ms] system. Upon production of such animal, the blastocyst can be used to produce thymus from other animal species by injecting respective PSCs. In this study, Cas9 cDNA was knocked-in under the control of the *Foxn1* promoter, a thymus-specific gene. Upon the expression of Cas9 and the ubiquitous expression of sgRNA[ms], cell ablation was hypothesized to occur in the thymus-specific cell lineage.

Chapter 2 – Materials and Methods

2.1 Animals

Animal handling, breeding, and experimental procedures were conducted under specific-pathogen-free (SPF) facilities in NAIST, according to the "Regulations and By-Laws of Animal Experimentation at the Nara Institute of Science and Technology". ICR mouse, B6D2F1 mouse, and C57BL6/J mouse used in this study were purchased from SLC, Japan, and maintained in NAIST Animal Facility.

2.2 ESC culture

Mouse ESC (mESC) lines used in this work were established from 129X1/B6J F1 (mF1-05; our laboratory original) and C57BL/6N (EGR-101; kindly provided by Dr. M Ikawa at Osaka University) mice. Rat ESC (rESC) line with constitutive EGFP expression[77] (rG104) was used to generate interspecies chimera (Kindly provided by Dr. M Ikawa at Osaka University). All cells were incubated at 37°C, under a 5% CO_2 condition. All cultured mESCs were cultured on gelatin-coated dishes, layered with mitomycin-C treated mouse embryonic fibroblast (MMC-MEF) or MMC-SNLP (puromycin resistant) as feeder cells in feeder media (FM). mESCs were seeded onto feeder cells that were cultured overnight.

mF1-05 at passage numbers P9 to P10 were used for *in vitro* experiments and cultured with ESC media (ESM). mESCs used for establishing mouse lines were cultured in N2B27-a2i/L (a2i) media. Culture media used in this research were listed in Table 1-Table 4.

Table 1: Basal media components

Basal media (BM) components	Manufacturer	Catalogue no.	Final concentration
DMEM (High Glucose)	Nacalai Tesque	08459-64	$1\times$
Sodium pyruvate	Thermo Fisher	11360070	1 mM
Non-essential amino acid	Thermo Fisher	11140050	1%
β-mercaptoethanol	Thermo Fisher	21985023	0.1 mM
Penicillin-Streptomycin	Thermo Fisher	15140122	0.1 mM

Table 2: Feeder media components

Feeder media (FM) components	Manufacturer	Catalogue no.	Final concentration
Basal media	-	-	-
Fetal Bovine Serum (FBS)	Biowest	S1650-500	10%

Table 3. ES media components

ESC Media (ESM) components	Manufacturer	Catalogue no.	Final concentration
DMEM (High Glucose)	Nacalai Tesque	08459-64	$1\times$
Sodium pyruvate	Thermo Fisher	11360070	1 mM
Non-essential amino acid	Thermo Fisher	11140050	1%
β-mercaptoethanol	Thermo Fisher	21985023	0.1 mM
Penicillin-Streptomycin	Thermo Fisher	15140122	0.1 mM
Mouse leukemia inhibitory factor (LIF)	NPO for Biotechnology Research and Development	-	1000 U/mL
Fetal Bovine Serum (FBS)	Biowest	S1650-500	20%

Table 4. a2i/L media components

N2B27-a2i/L components	Manufacturer	Catalogue no.	Final concentration
KnockOut^{TM} DMEM/F12	Thermo Fisher	12660012	$0.5\times$
Neurobasal^{TM} Medium	Thermo Fisher	21103049	$0.5\times$
N2 supplement	Thermo Fisher	17502001	$0.5\times$
B-27 Supplement	Thermo Fisher	17504001	$0.5\times$
L-glutamine	Thermo Fisher	25030081	2 mM
β-mercaptoethanol	Thermo Fisher	21985023	0.1 mM
Penicillin-Streptomycin	Thermo Fisher	15140122	0.1 mM
CHIR99021	Axon	CT99021	3 µM
CGP77675	Sigma	SML0314	1.5 µM
Mouse leukemia inhibitory factor (LIF)	NPO for Biotechnology Research and Development	-	1000U/mL

Table 5: 2i/L media components

N2B27-2i/L components	Manufacturer	Catalogue no.	Final concentration
KnockOut™ DMEM/F12	Thermo Fisher	12660012	0.5×
Neurobasal™ Medium	Thermo Fisher	21103049	0.5×
N2 supplement	Thermo Fisher	17502001	0.5×
B-27 Supplement	Thermo Fisher	17504001	0.5×
L-glutamine	Thermo Fisher	25030081	2 mM
β-mercaptoethanol	Thermo Fisher	21985023	0.1 mM
Penicillin-Streptomycin	Thermo Fisher	15140122	0.1 mM
CHIR99021	Axon	CT99021	3 µM
PD0325901	Wako	168-25293	1 µM
hLIF	Sigma	MFCD00163950	0.2ng/mL
Mouse leukemia inhibitory factor (LIF)	NPO for Biotechnology Research and Development	-	1000U/mL

2.3 Design and construction of sgRNA^{ms}

pSpCas9(BB)-2A-Puro (PX459) V2.0 was purchased from Addgene (plasmid #62988)[32]. Two sgRNA that can recognize multiple sites (sgRNA^{ms}) in genomes of different species were designed to induce cell ablation, namely sgRNA^{ms1} and sgRNA^{ms2} (Table 6). The number of sites targeted by sgRNA^{ms} was analyzed using CRISPRdirect software[78]. These sgRNA^{ms} were ligated at the BbsI site of PX459 individually, producing PX459-sgRNA^{ms1} and PX459-sgRNA^{ms2}.

Table 6. Sequence of sgRNA^{ms} and number of target sites

sgRNA	Sequence information (5' – 3')	Number of target site(s)			
		Mouse	Rat	Pig	Human
sgRNA^{ms1}	AGGAAGGAAGGAAGGAAGGA	181,903	56,876	21,151	36,251
sgRNA^{ms2}	TGGATGGATGGATGGATGGA	22,314	26,853	3,783	12,711

2.4 Validation of designed sgRNA^{ms}

To confirm the cleavage activity of the Cas9-sgRNA^{ms} complex, targets for both sgRNA^{ms} were constructed on pCAG-EGxxFP, kindly provided by Dr. M Ikawa at Osaka University (Addgene plasmid #50716)[79]. Plasmids PX459-sgRNA^{ms} and respective targets were transfected to HEK293T cells cultured in FM. Cells were observed 48 hours later for EGFP signal from target plasmid as an indicator of successful cleavage and recombination of EGFP cassette.

2.5 Establishment of inducible Cas9-T2A-EGFP with hU6-sgRNA[ms] HEK293T cells

To induce Cas9-EGFP expression in HEK293T cells, Tet-One[TM] doxycycline-inducible system from Takara Bio (Japan) was used with some modifications[80]. DNA cassettes of CAG-TetOn3G-T2A-Puro[R] and TRE3Gs-Cas9-T2A-EGFP were constructed and ligated into a piggyBac vector, between two inverted terminal repeats (ITRs), to produce the final plasmid (Figure 9). Hyperactive piggyBac transposase was used to paste gene sequence between PB5 and PB3 sequence into TTAA sites across the genome[81]. Inducible Cas9-EGFP plasmid and pCMV-hyPBase plasmid (kindly provided by Dr. K Yusa at Sanger institute) were simultaneously transfected to HEK293T cells. Puromycin selection (0.5µg/mL) was conducted for 7 days on transfected cells. Surviving cells were induced with Doxycycline (1.5µg/mL) for 3 days and observed for EGFP signal under a fluorescent microscope.
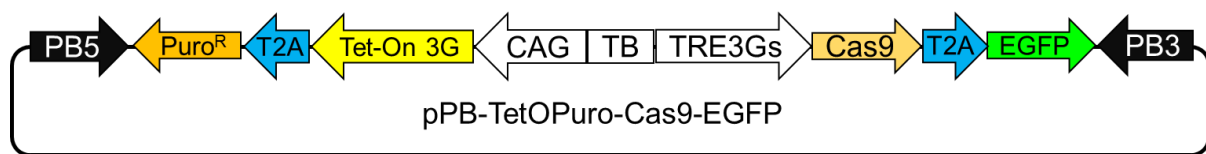
Figure 9. Map of the doxycycline-inducible Cas9-T2A-EGFP plasmid. TB: transcription blocker; TRE3Gs: Doxycycline transactivating promoter.

Briefly, the CAG promoter is constitutively expressed, and transgenic cells can be screened with puromycin. In the absence of doxycycline, Tet-On 3G protein does not exert any effect on the cells; however, in the presence of doxycycline, Tet-On 3G protein binds to doxycycline and transactivates TRE3Gs promoter. Expression of Cas9 can be monitored by EGFP signal after doxycycline induction. Single cells with a strong EGFP signal were isolated to establish a homogeneous transgenic cell line. Next, inducible Cas9-T2A-EGFP cell lines were used to establish stable transgenic cell lines expressing hU6-sgRNA[ms] by hygromycin (300µg/mL) selection for 7 days. These inducible Cas9-EGFP HEK293T cells with sgRNA[ms] were used for subsequent experiments.

2.6 Establishment of knock-in cell lines

CRISPR-Cpf1 was used to induce double-strand break for the knock-in of sgRNA-expressing DNA cassette or Cas9 cDNA cassette on mESCs via Cpf1-expressing vector, pTE4398 (Addgene plasmid #74042)[82]. The crRNA used for Cpf1 recognition sites was ligated to the BsmBI site of pTE4398. The crRNA target sites by Cpf1 and respective oligonucleotide sequences were listed in Table 7 (PAM sequences in red).

Table 7. crRNA targeting sequences for gene knock-in by CRISPR-Cpf1 system

Locus	crRNA sequence (5' – 3')
Rosa26	**TTTC**TAGAAGATGGGCGGGAGTCT
Foxn1	**TTTC**TTCGAGGCCAGGACTGGGTG
Foxn1^{Cas9}	**TTTG**CCCCTCCCCCGTGCCTTCCT
Foxn1-3'UTR	**TTTA**AGGTGAGCCCAATATGGGGC

All knock-in targeting vectors were constructed on pLSODN-4D or pUC19 backbone, consisting of knock-in genes flanked by left and right homologous arms (Figure 10). PCR primers used for homologous arms amplification were listed in Table 8. Both pTE4398 and the targeting vectors were transfected to mouse ESCs using Lipofectamine 3000 (Thermofisher). G418 (150µg/mL) selection was conducted for 3 days in a2i media. Colonies were picked up and screened for knock-in by genotyping and sequencing. PCR primers for genotyping and sequencing were listed in Table 9.
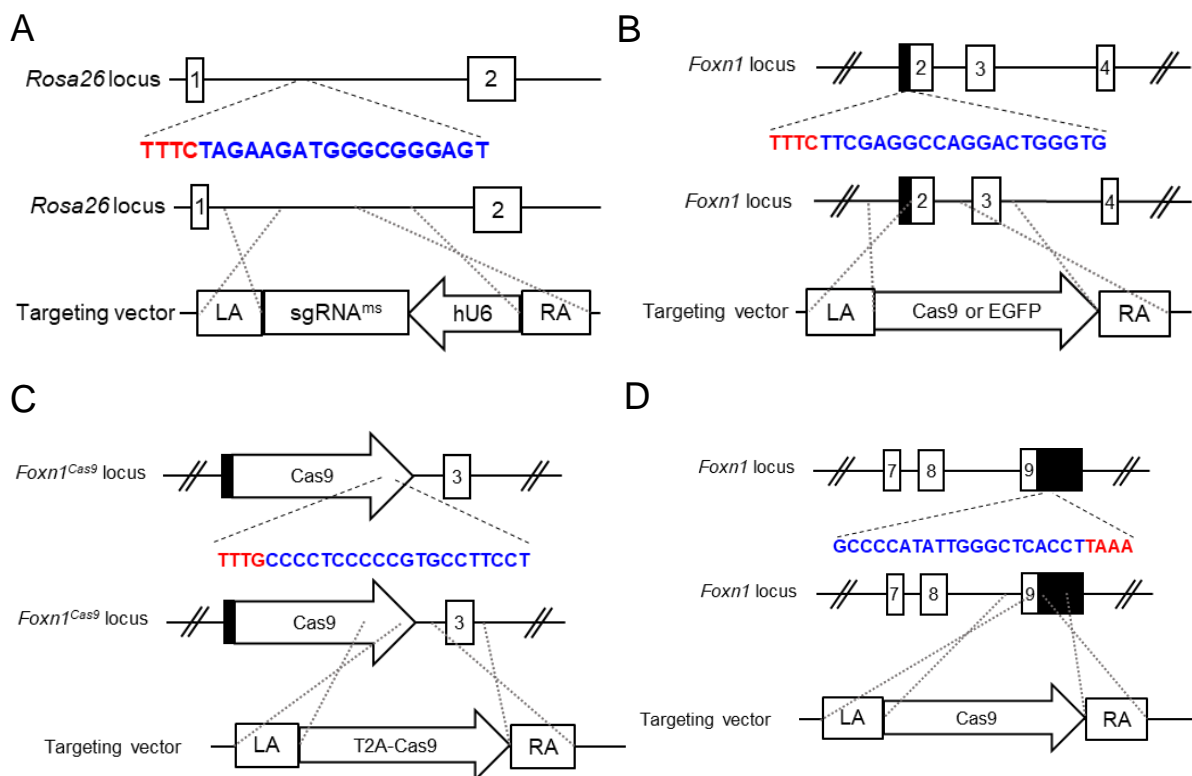
Figure 10. Schematic diagram of knock-in strategy at different loci. (A) *Rosa26_ms*; (B) *Foxn1*^{Cas9}; (C) *Foxn1*$^{Cas9-T2A-Cas9}$; and (D) *Foxn1-3' UTR*^{Cas9}. Red: PAM sequence of *CpfI*; Blue: crRNA sequence; LA: Left homologous arm; RA: Right homologous arm.

**Table 8. Primers to amplify homologous arms on targeting vector construction**

PCR product	Primer name	Sequence (5' – 3')
Foxn1 left arm	Foxn1-Left-FW	TGCCTGCAGGCTCTTCGATCTGTGTGCT TGTGCTGTGCTC
	FoxN1-Left-RV (SNP)	TCCTGGCCTCGAAGATAGCC
Foxn1 right arm	FoxN1-Right-FW (SNP)	GCTATCTTCGAGGCCAGGAACGCGTTA GACCCAGAAGGGCCAAGT
	Foxn1-Right-RV	TGGCAATGCCCGGGATGATTGCATAGG GGTGTGTTGGTC
Rosa26 left arm	Rosa26-left_F	ATGCCTGCAGGCTCTTCGATGAGAAGG GAGCGGAAAAGTC
	MluI+Rosa26-left-R	ACGCGTGACTGGAGTTGCAGATCACGA GGG
Rosa26 right arm	MluI+Rosa26-Right-F	TGCAACTCCAGTCACGCGTGGAATTGA ACAGGTGTAAAATTGG
	Rosa26-Right_R	TGGCAATGCCCGGGATGATAATGCCAT GAGTCAAGCCAG

Table 9. Primers for genotype determination of knock-in mESCs and mouse lines

Locus	Primer name	Sequence (5' – 3')
Rosa26	Rosa26 indel check FW	AGCTGCAGTGGAGTAGGCGG
	Rosa26 indel check RV	TGGAAAATACTCCGAGGCGG
Foxn1	FoxN1 Left FW seq2	GGTTACCCTCTGTGTCATTG
	FoxN1 Right RV seq2	GGAGTTTATTGCACCAAGCC
Foxn1^{Cas9}	FoxN1-GFP Geno FW	CCAAAACTGAGCACAAAGGT
	Cas9 seq R1	AACAGGTCGGCGTACTGGTC
Foxn1^{EGFP}	GFP Rv seq primer 1	AACTTGTGGCCGTTTACGTC
Foxn1$^{Cas9-T2A-Cas9}$	Cas9 seq F5	GAACCGCCCTGATCAAAAAG
Foxn1-3' UTR^{Cas9}	Foxn1 3' UTR LA seq F	GTTCAGTGATTACTTGAGGT
	Foxn1 3' UTR RA seq R	GTAGGCTTTAAGGGTGTAAG
	Foxn1_int8 F	GGGTCAATACCCCAGCATCA

2.7 Establishment of *p53-KO* cell lines

Cas9 was used to knock out *p53* in mF1-05 mESCs using the sgRNA listed in Table 10 (PAM sequence in red). All sgRNA were cloned into the *BbsI* site of PX459. Cells were transfected with *p53*-sgRNA and selected with puromycin (1µg/mL) for 2 days. Primers used for genotyping were shown in Table 11. The schematic diagram shows the location of sgRNAs and primers relative to the *p53* locus (Figure 11).
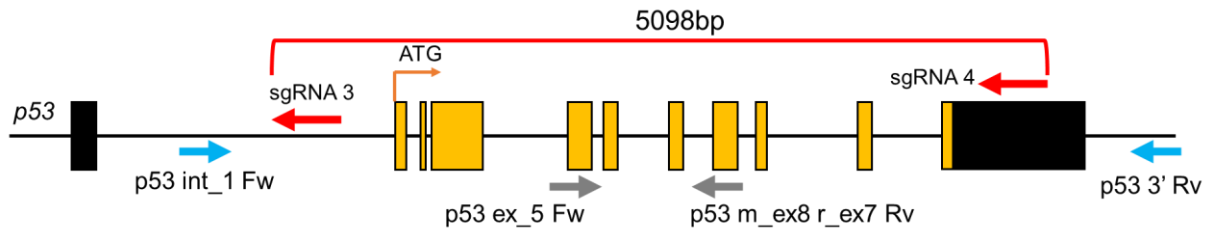
Figure 11. Schematic diagram of mouse *p53* locus with sgRNAs and primer location

Table 10: Cas9-sgRNA sequences for *p53* KO

sgRNA name	sgRNA sequence (5' – 3')
m_*p53*-sgRNA3	ATTTCAGGAAACTTATGCGA**GGG**
m_*p53*-sgRNA4	CTGGCTGGATAGAATTTCGC**TGG**

Table 11: Primers for *p53* genotyping and RT-PCR

Primer name	Sequence (5' – 3')
p53 int_1 Fw	GGGTTTGAAGAATGGAGCTG
p53 3' Rv	TGCAGCCCACAGACTGA
*p53 ex_5 Fw	CCATGGCCATCTACAAGAAGT
*p53 m_ex8 r_ex7 Rv	AACACGAACCTCAAAGCTGTC

Primers used for genotyping PCR and RT-PCR.

2.8 DNA sequencing

BigDye™ Terminator v3.1 Cycle Sequencing Kit (Applied Biosystems) was used for DNA sequencing and cycle sequencing was conducted according to the manufacturer's protocol. PCR product was subjected to ethanol/EDTA precipitation and DNA sequences were analyzed with ABI PRISM 3100 Genetic Analyzer (Applied Biosystems).

2.9 Karyotyping

Before the generation of a chimera from injection to embryos, the chromosomes of mESCs were analyzed. mESCs were cultured until confluent on a gelatin-coated dish in ESM. KaryoMAX® COLCEMID® (Gibco) was added to the cells at a final concentration of 100 ng/mL and incubated for 3 hours. mESCs were dissociated into single-cell suspension with 0.25% trypsin. Cells were then subjected to hypotonic treatment with 1% sodium citrate solution for 5 minutes, followed by fixation with fixing solution (1-part acetic acid and 3-parts methanol). Fixed cells were dropped on a microscope slide glass and visualized under a

microscope (EVOS® FL, Invitrogen). Chromosome numbers were counted. Cell lines with normal chromosome numbers (40 chromosomes) in more than 60% of counted cells were used to establish mouse lines.

2.10 Validation of sgRNA^{ms} function in mESCs

To validate the functionality of sgRNA^{ms}, plasmid PX459 expressing Cas9-T2A-Puro^R and sgRNA^{ms} were stably transfected into mESCs. Cells were selected with puromycin (1µg/mL) for seven days. The remaining cells were stained with alkaline phosphatase (ALP) to detect surviving mESCs. The number of colonies larger than 1mm^2 was counted and tabulated.

2.11 Alkaline phosphatase (ALP) staining

ALP staining was carried out using a Histofine alkaline phosphatase staining kit (Nichirei Bioscience, Japan), according to the protocol provided by the manufacturer. Cultured cells were washed twice in PBS and fixed with an equal volume of 4% paraformaldehyde (PFA) as to cell culture media. Cells were fixed for 5 minutes at room temperature, followed by washing with PBS twice. Freshly prepared ALP staining regent was then added to fixed cells and stained for at least 30 minutes until a purplish-pink signal was observed. Cells were washed with double-distilled water prior to imaging with a digital camera (COOLPIX P7100, Nikon) or observed under a stereomicroscope.

2.12 Prediction of cell death caused by Cas9-sgRNA^{ms} system

An equal number (1×10^5) of WT and *Rosa26_ms* mESCs were seeded and transfected with pCAG-tdTomato-T2A-Puro^R or pCAG-Cas9-T2A-Puro^R. Puromycin (1µg/mL) was added for 3 days, and cells were analyzed using flow cytometry. The number of SSEA1$^+$ and tdTomato$^+$ cells were counted using flow cytometry and predicted cell death was calculated (Table 12 and Equation 1-Equation 3). This experiment was repeated three times and statistical analysis was conducted.

Table 12. Matrix tabulating cell number of different experimental conditions

Mouse ESC lines	Number of SSEA1$^+$ cells	
	pCAG-Cas9	pCAG-tdTomato
WT	(A)	(B)
Rosa26_ms1(pT-) *Rosa26_ms2(pT-)*	(C)	(D)

$$Ratio\ of\ surviving\ cells = \frac{B}{A} = \alpha \qquad \textbf{Equation 1}$$

$$Speculated\ number\ of\ surviving\ cells = D \times \alpha = \beta \quad \textbf{Equation 2}$$

$$Predicted\ cell\ death\ percentage = \frac{\beta - C}{\beta} \times 100\% \quad \textbf{Equation 3}$$

2.13 Harvest of two-cell stage embryos

Female ICR mice aged between 8- to 10-weeks old were administered with 0.1 mL of CARD HyperOva® (Cosmo Bio) through intraperitoneal injection. After 48 hours, 7.5 IU of hCG was administered via a similar method. Superovulated mice were then subjected to mating with male ICR mice. The presence of a vaginal plug on the next morning indicates the occurrence of coitus and the age of the embryo was defined as embryonic day (E) 0.5. The female mice were sacrificed via cervical dislocation and E1.5 embryos were collected by flushing M2 media (Sigma) through the oviducts. Harvested embryos were cultured at 37°C, 5% CO_2 condition in KSOM media[83].

2.14 Generation of chimeric animals

Cultured mESCs were used to generate chimeric animals. mESCs were subjected to karyotyping to confirm the presence of normal chromosome number (40 chromosomes) before injecting into embryos. Cultured embryos of E2.5 at the 8-cell stage were injected with mESCs using Piezo-micromanipulator (PMAS-CT150, Prime Tech LTD) under a light microscope (DM-IRC-Leica). Each embryo was injected with six to eight mESCs in M2 media. The injected embryos were cultured until E3.5 in KSOM media and transferred to the uterus of E2.5 pseudopregnant mice (ICR x ICR) under general anesthesia. Embryos transferred to pseudopregnant mice were defined as E2.5.

To generate mouse←rat xenogeneic chimera, rG104 cells were injected into E3.5 mouse embryos of $Foxn1^{Cas9};Rosa26\_ms2$.

Generated animals were observed for EGFP signal under a fluorescent microscope (MZFL III, Leica).

2.15 Hematoxylin and eosin (H&E) staining

Harvested thymus was fixed in 4% paraformaldehyde/PBS overnight at 4°C followed by incubation in sucrose solution of increasing concentration (10%, 15%, 20%). The thymus was then embedded in Tissue-Tek® O.C.T™ compound (Sakura Finetek, Japan). The embedded thymus was then sectioned with cryostat NX70 (Thermo Fisher Scientific) at 10 µm and mounted on glass slides.

The glass slides were dried at 37°C for 2 hours and washed in PBS(-). Slides were immersed in Mayer's hematoxylin solution for 1 minute, followed by 5 minutes of washing in

ddH$_2$O. Then immersed in Eosin solution (1-part Eosin Y solution to 2-parts 80% ethanol, with 0.5 mL/100 mL acetic acid) for 3 minutes. The slides were washed twice in ddH$_2$O for 4 minutes each. The slides were then immersed in ethanol in increasing concentrations (70%, 90%, 100%), for 30 seconds at each concentration. Slides were then washed in xylene twice, at 30 seconds each. Entellan® (MERCK, Germany) was added to the slides and covered with a covered slip. The thymus section was then observed under microscopy (BX60, Olympus).

2.16　Immunostaining

Cells attached to glass coverslip or tissue section in O.C.T. compound were used for immunostaining. Samples were washed twice in 2mL PBS(-) and fixed in 2% paraformaldehyde (Nacalai Tesque) for 5 minutes. Next, samples were dehydrated with acetone (Nacalai Tesque) for 5 minutes. Permeabilization was carried out in 50μL of 0.5% Triton X-100 (Nacalai Tesque) for 5 minutes. Samples were then blocked with 10% goat serum (143-06561, Wako) in BlockAce solution (KAC Co., Ltd.) at room temperature for 1 hour, followed by washing in 0.1% BSA/PBS (Sigma) twice, for 5 minutes each. Primary antibody staining was conducted at 4ºC, overnight in humid conditions. Secondary antibody staining was conducted at room temperature for 1 hour. Nuclei were stained with Hoechst33342 (1:1000; KV072, Wako) for 3 minutes before imaging. All immunostaining antibodies used in this research were listed in Table 13.

Table 13. List of antibodies used in immunostaining

Antibody	Company	Catalogue number	Working concentration
Anti-mouse γH2AX	Biolegend	613402	1:50
Anti-mouse K8	Biolegend	904804	1:50
Anti-mouse, anti-rat K5	Biolegend	905504	1:50
Anti-BrdU	Bio-Rad	OBT0030	1:100
Anti-GFP	MBL	COD598	1:50
AlexaFluor555 anti-mouse IgG	Invitrogen	A21425	1:1000
AlexaFluor647 anti-rat IgG	ABCAM	ab150159	1:1000
AlexaFluor647 anti-rabbit IgG	Invitrogen	A21246	1:1000

2.17   MTT assay

Inducible Cas9-EGFP HEK293T cells were seeded at a density of 5 x 10^3 cells/well on 96 well plates coated with 0.2% Matrigel in basal media. Cells were induced with doxycycline (1.5 µg/mL) for 72 hours prior and an MTT cell count kit (Nacalai Tesque, 23506-80) was used to perform the MTT assay. Cells were treated with 10µL of MTT solution and incubated for 3 hours at 37°C, followed by adding 100µL of solubilization solution and incubated overnight at 37°C. Absorbance at 595nm was measured with a reference reading at 620nm, using a multi-mode plate reader (Berthold, TriStar LB942). The cell proliferation rate was calculated using the following formula:

$$Cell\ proliferation\ rate\ (\%) = \frac{A_{595}\ Dox^+}{A_{595}\ Dox^-} \times 100\%$$

2.18   DNA synthesis assay

Doxycycline-inducible Cas9-EGFP HEK293T cells were cultured in a 6-well plate and attached to a glass coverslip. After 48 hours of doxycycline induction, then BrdU was added to the culture at a final concentration of 10µM and further incubated for another 24 hours. Cells were washed briefly in cold PBS(-). 1mL of 1x cytofix/cytoperm buffer in PBS was added to the cells and incubated at room temperature for 30 minutes. Buffer was removed and cells were washed once with 1mL of wash buffer. 1mL of cytoperm plus buffer was added and incubated on ice for 10 minutes. Buffer was then removed and added with 1mL of 1x cytoperm/cytofix buffer in PBS and incubated at room temperature for 5 minutes. Buffer was removed and washed with 1mL wash buffer. Coverslips were gently removed from the 6-well plates with fine-tipped forceps and cells were treated with 50µL of 0.3mg/mL DNaseI in PBS at 37°C for 1 hour. Cells were washed twice with wash buffer at room temperature. Primary antibody staining was conducted in 0.1% BSA/PBS on ice for 30 minutes. Cells were washed in wash buffer prior to secondary antibody staining in 0.1% BSA/PBS on ice for 20 minutes. Lastly, nuclei were stained with Hoechst33342 (1:1000; KV072, Wako) for 3 minutes before imaging. All reagents used were listed in Table 14.

Table 14. Reagents used in DNA synthesis assay

Solution	Components	Volume
2x cytofix/cytoperm buffer	4% PFA	45mL
	2% saponin	5mL
Wash buffer	FBS	2.5mL
	20x PBS	2.5mL
	2% saponin	2.5mL
	ddH$_2$O	42.5mL
Cytoperm plus buffer	BlockAce solution	2.5mL
	5% Triton-X 100	5mL
	20x PBS	2.5mL
	ddH$_2$O	40mL

2.19 Flow cytometry

HEK293T and mESCs cells were treated with 0.1% - 0.25% trypsin and harvested. Cells were centrifuged at 4ºC, 2,000x g for 5 minutes, and the supernatant was removed. PBS(-) was used to resuspend cells and centrifuge was repeated. The supernatant was removed and proceeded with staining with annexin V and propidium iodide in 1x Annexin-V staining buffer (10mM HEPES, 140mM NaCl, 2.5mM CaCl$_2$), at 4ºC for 30 minutes. Samples were topped up with 450µL ice-cold PBS(-) and filtered through 37µm mesh before cytometry analysis.

Thymus and spleen from P9 mice were harvested in chilled PBS(-) and mashed between glass slides to obtain thymocytes and splenocytes. Cells were resuspended and washed in fresh cold PBS(-). 1x RBC lysis was carried out by incubation on ice for 5 minutes. Cells were stained for CD45, CD3, CD8, and CD4 to determine the T cell population in total lymphocytes in 50µL of 0.1% BSA/PBS, at 4ºC for 30 minutes. Samples were resuspended in 500µL of 0.1% BSA/PBS and filtered through 37µm mesh before cytometry analysis.

A suitable amount of cell suspension was analyzed using BD Accuri C6 Flow Cytometer (Becton Dickinson) and FlowJo software (Becton Dickinson).

Table 15. List of antibodies or markers used in flow cytometry

Antibody/Marker	Company	Catalogue number	Working concentration
AlexaFluor647 Annexin-V	Biolegend	640912	1:50
Propidium iodide	Wako	341-07881	1μg/mL
SSEA1	R&D Systems	MAB2155	1:100
AlexaFluor 488 anti-mouse IgM	Biolegend	A21042	1:500
APC anti-mouse CD45	Biolegend	100516	1:50
PE anti-mouse CD3ε	Biolegend	100308	1:50
APC anti-mouse CD4	Biolegend	100516	1:50
PerCP anti-mouse CD8a	Biolegend	100732	1:50

2.20   RNA analysis

The thymus harvested from pups of 9-days post-partum (P9), HEK293T cell lines, and mESCs were subjected to RNA extraction using TRIzol™ Reagent (Invitrogen, 15596026). Briefly, the thymus was harvested in chilled PBS(-). The homogenized tissue was added with 1mL TRIzol reagent per 100mg tissue. The RNA was extracted with chloroform and isopropanol, followed by precipitation using 70% ethanol, and finally resuspended in DEPC-water.

The extracted RNA was first treated with recombinant DNase I (Takara Biotechnology, 2270A), followed by phenol-chloroform precipitation.

Reverse transcription was conducted with SuperScript™ III First-strand synthesis system (Invitrogen, 18080-051) and SuperScript™ IV Vilo Master Mix (Invitrogen, 11756050) according to the manufacturer's protocol. Starting amount of RNA was measured and adjusted across all samples for downstream cDNA synthesis.

RT-PCR targets and primers were shown in Table 16. PCR conditions were as follows: initial denaturation at 95°C for 5 minutes; 40 cycles of 95°C for 30 seconds, Tm at 30 seconds, 72°C for 1 minute/kb; final elongation at 72°C for 7 minutes; and hold at 16°C indefinitely.

Table 16. Primers for RT-PCR

Target product	Primer name	Sequence (5' – 3')
Cas9	Cas9 seq F5	GAACCGCCCTGATCAAAAAG
	Cas9 seq F7	CTGAGCGAACTGGATAAGGC
	Cas9 seq R4	GCCCTTATCCCACACGATCT
sgRNA^{nt} or sgRNA^{ms}	sgRNA^{nt}_Fw	CGGGTCTTCGAGAAGACCT
	sgRNA^{ms1} Fw	CACCAGGAAGGAAGGAAGGAAGGA
	sgRNA^{ms2} Fw	CACCTGGATGGATGGATGGATGGA
	sgRNA scaffold Fw	GACTCGGTGCCACTTTTTC
mGAPDH	GAPDH-F for qPCR	CCAGTATGACTCCACTCACG
	GAPDH-R for qPCR	GACTCCACGACATACTCAGC
mEpCAM	mEpCAM_ex2-3_F	GCTCAGAGAGACTGTGTCTG
	mEpCAM_ex4-5_R	ATGATCCAGTAGGTCCTCAC
hGAPDH	hGAPDH_ex3-4_F	CCTCAACTACATGGTTTACA
	hGAPDH_ex7-8_R	GGACTGTGGTCATGAGTC

2.21 Protein extraction and western blot analysis

Thymus from P9 mice was harvested and protein lysate was prepared in RIPA buffer (Nacalai, 08714) according to the manufacturer's protocol. Protein samples were extracted by freeze-thaw method with liquid nitrogen. Samples were weighed and 3mL of 1x RIPA buffer was added to 1g of samples before homogenization. The protein amount was measured using a BCA protein assay kit (Nacalai, 06385-00). An equivalent amount of protein sample was separated using 4-12% Bolt Bis-Tris gel (Invitrogen, NW04120BOX). Gel electrophoresis was conducted in 1x SDS running buffer (Invitrogen, B0002) at a constant voltage of 200V for 30 minutes. After gel electrophoresis, proteins were transferred to immobilon-P PVDF membrane (Merck, IPVH00010) in transfer buffers at a constant voltage of 25V for 40 minutes. The membrane was blocked in 5% skim milk powder (Wako, 190-12865) dissolved in 0.05% Tween-20/PBS (PBS-T). The membrane was incubated with a primary antibody in 1% skim milk at 4ºC, overnight. Subsequently, the membrane was washed in PBS-T and incubated with a secondary antibody conjugated with horseradish peroxidase in 1% skim milk and incubated at room temperature for 1 hour. Peroxidase activity was detected with Chemi-Lumi One (Nacalai, 07880) and visualized using FUSION-Chemiluminescence Imaging System (Vilber-Lourmat). All primary and secondary antibodies in the western blot were listed in Table 17.

Table 17. Antibodies used in western blot

| Antibody/Marker	Company	Catalogue number	Working concentration
Anti-Cas9	Takara	632607	1:500
Anti-EpCAM	Proteintech	21050-1-AP	1:500
HRP-linked anti-rabbit IgG	Cytiva	NA934	1:1000

2.22 Statistical analysis

All statistical tests in this study were conducted with Prism 9 (Graphpad) software. The confidence interval was set at 95%, and a p-value less than 0.05 indicates a significant difference between the compared datasets.

Chapter 3 – Results

3.1   Validation of Cas9-sgRNA^{ms} cleavage action in HEK293T

HEK293T cells were transfected with Cas9-sgRNA^{ms} expressing plasmid and sgRNA^{ms} target sequence that is present in pCAG-EGxxFP. Expression of EGFP signifies sgRNA^{ms} target was successfully cleaved and homologous recombination had occurred (Figure 12).
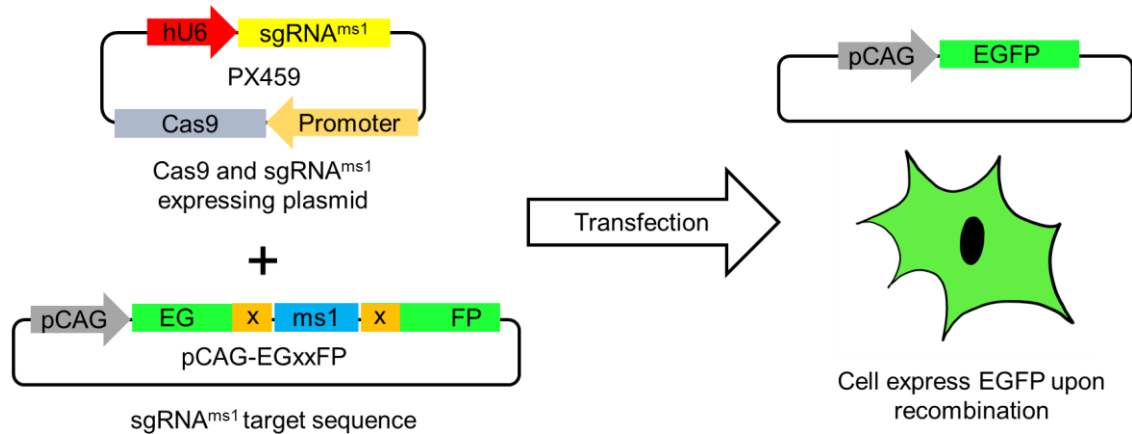

Figure 12: Schematic diagram of experiment outline and concept to test the specificity of Cas9-sgRNA^{ms}

48 hours after transfection, a strong EGFP signal was observed, suggesting that both sgRNA^{ms1} and sgRNA^{ms2} successfully cleaved their targets *in vivo*, as compared to the low EGFP level in negative controls, transfected with only sgRNA^{ms} target sequence (Figure 13A). The target sequence of *Cetn1* and PX459_sgRNA-*Cetn1* was used as positive control[79]. Furthermore, cells transfected with Cas9-sgRNA^{ms1} plasmid and sgRNA^{ms2} target sequence, and vice versa, showed similar EGFP signal compared to negative controls (Figure 13B). This suggests that both designed sgRNA^{ms1} and sgRNA^{ms2} could only recognize and cleave their respective target sequences, and there was no cross recognition between the two sgRNA^{ms}.
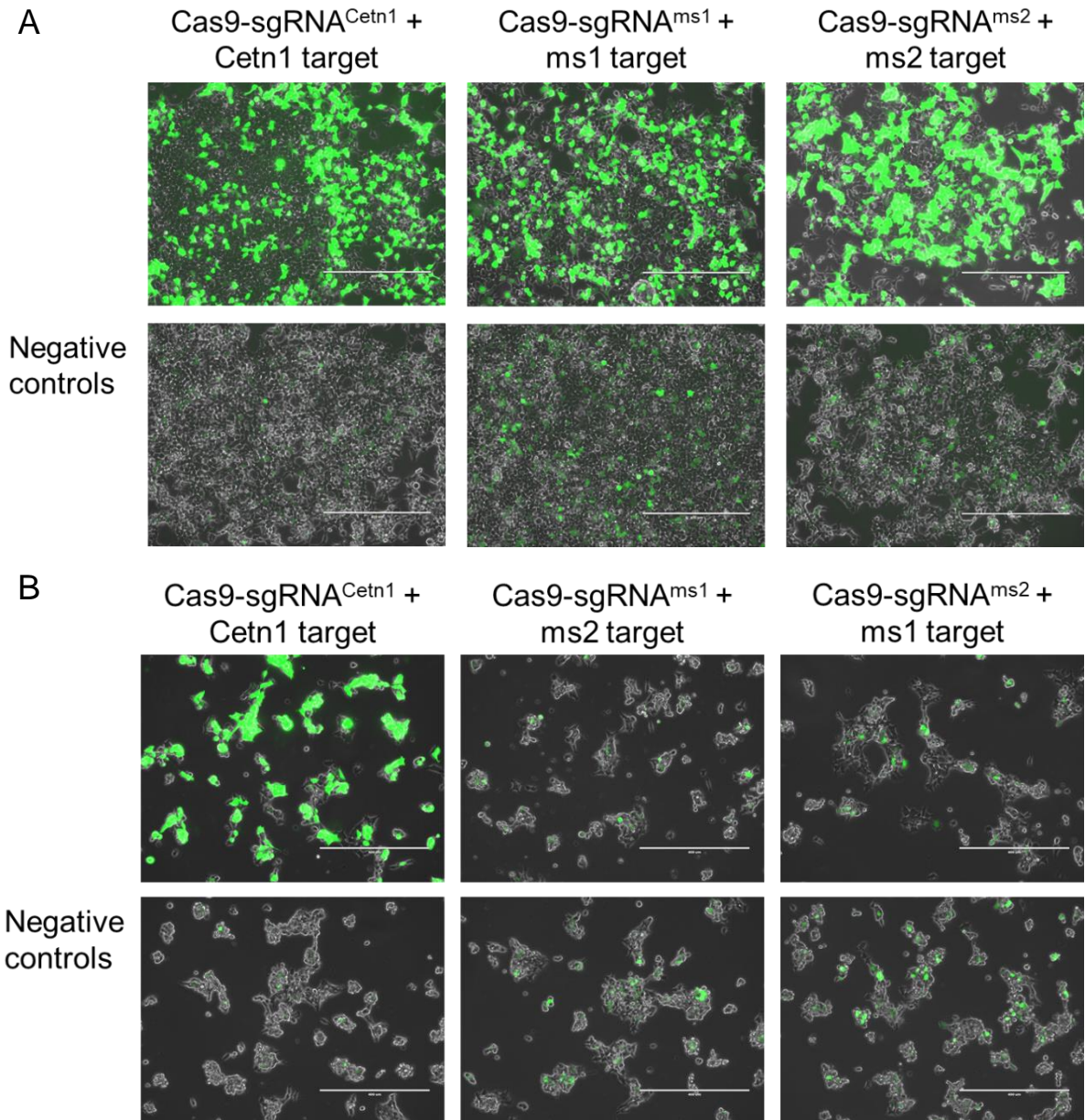
Figure 13. Successful cleavage of ms1 and ms2 target sequence by Cas9 indicated by the EGFP expression in cultured HEK293T cells. (A) A strong EGFP signal was observed 48 hours after transfection. Scale bar: 400µm. (B) A minimal EGFP signal was observed when sgRNA^{ms1} was transfected with the sgRNA^{ms2} target sequence and vice versa. Scale bar: 400µm.

3.2 Functional analysis of Cas9-sgRNA^{ms} in HEK293T

Before applying the Cas9-sgRNA^{ms} system to generate organ-deficient animal models, the downstream effects of Cas9-sgRNA^{ms} were investigated using HEK293T cells. To investigate if cell death was induced, HEK293T cells were transiently transfected with plasmids expressing Cas9-T2A-EGFP under the control of the Cbh promoter, with or without sgRNA^{ms}. At different time points after the transfection, cells were harvested and stained with cell death markers, Annexin-V (AxV), and propidium iodide (PI). After staining, cells were analyzed with flow cytometry. Surviving cells are AxV and PI double negative (AxV$^-$/PI$^-$),

cells in early apoptosis are AxV single positive (AxV$^+$/PI$^-$) and the cells in late apoptosis or necrosis are AxV and PI double positive (AxV$^+$/PI$^+$).

The presence of the EGFP signal signifies positively transfected cells. EGFP$^+$ cell number on day 2 after transfection was used as the baseline to calculate the relative number of cells transfected with different plasmids on subsequent days. Results showed that the relative EGFP$^+$ cell number in the presence of sgRNA^{ms1} and sgRNA^{ms2} were significantly lower on day 3 and day 4 (Figure 14). This shows that Cas9-sgRNA^{ms} inhibited the growth of HEK293T cells.
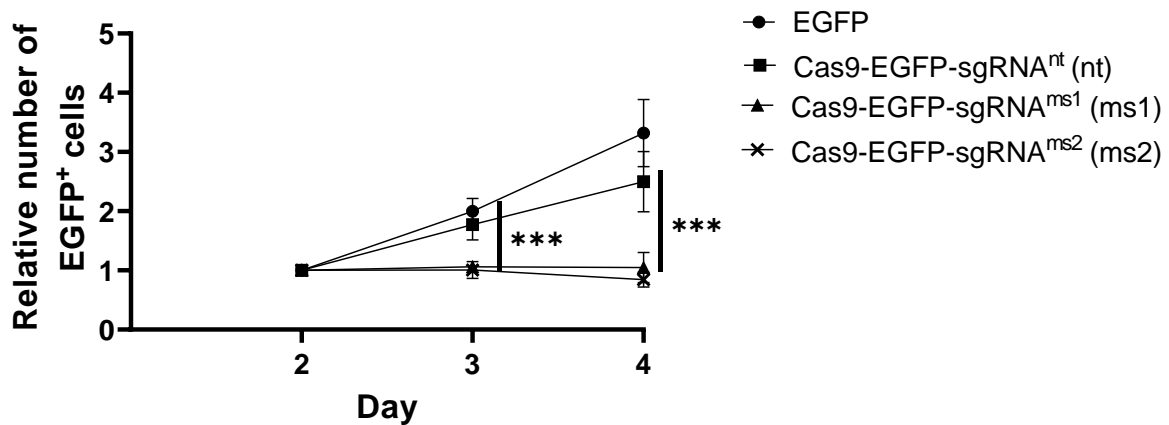
Figure 14. The average relative number of EGFP$^+$ cells in each transfection condition, across day 2 to day 4 after transfection. Mean ± S.D. Statistical analysis: Student's *t*-test, ***$p<0.001$.

EGFP$^+$ cells were gated and analyzed for AxV and PI staining to evaluate the apoptosis status. To rule out cell death due to Cas9 only, relative cell population was computed by comparing data to the cells transfected with Cas9-EGFP at each time point. Results showed that there was a significant increase in relative cell population in the early and late apoptosis stage in cells expressing Cas9-EGFP-sgRNA^{ms1} and Cas9-EGFP-sgRNA^{ms2}. This was observed from day 3 to day 4 after transfection (Figure 15).
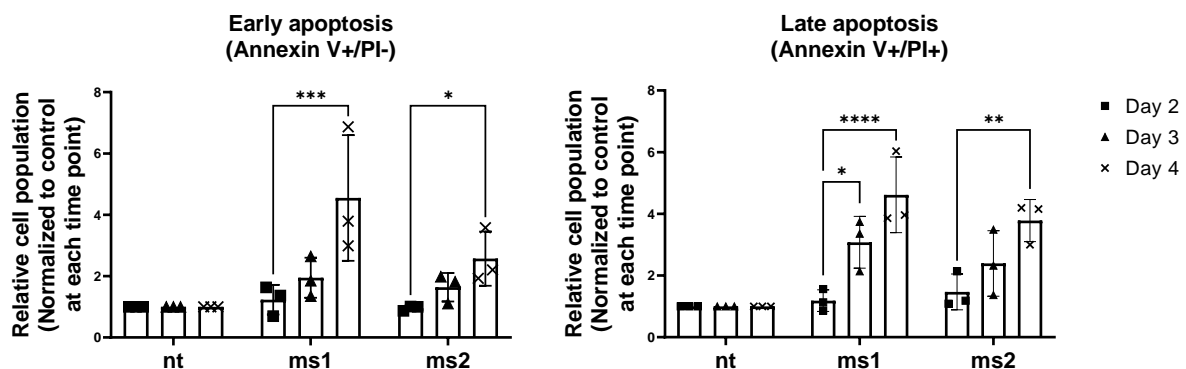
Figure 15. Significant increase in relative early and late apoptotic cell population at different time points after transfection of indicated plasmids. Mean ± S.D. Statistical analysis: Two-way ANOVA, *$p<0.05$, **$p<0.01$, ***$p<0.001$, ****$p<0.0001$.

3.3 Investigation of cellular defects by Cas9-sgRNA^{ms} using inducible Cas9-EGFP HEK293T cell lines

To eliminate the transfection efficiency difference between individual cells, homogenous doxycycline-inducible Cas9-EGFP cell lines were established on HEK293T cells using the piggyBac transposon system (schematic diagram in Figure 9). Upon doxycycline treatment for 48 hours, the EGFP signal was observed, suggesting the expression of Cas9 (Figure 16A). Cell lines were analyzed with flow cytometry and clones with high EGFP expression levels were identified and used for subsequent experiments (Figure 16B).
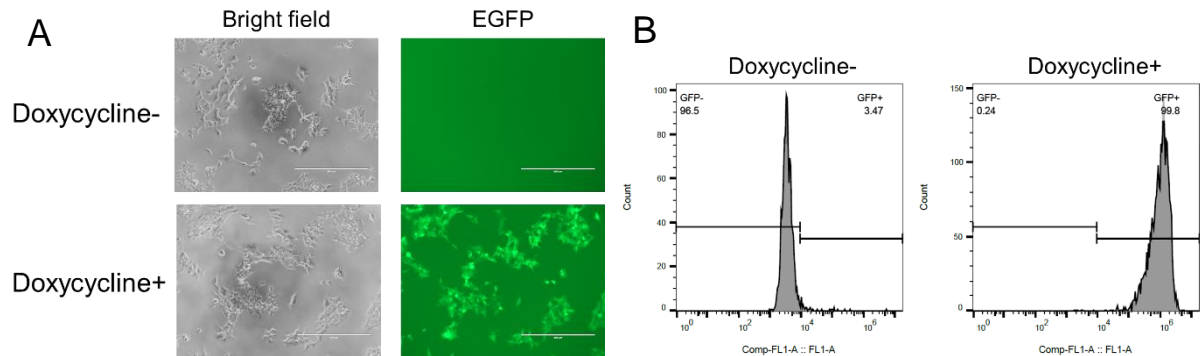
Figure 16. Homogenous transgenic HEK293T lines expressing EGFP after 48 hours of doxycycline treatment. (A) Strong EGFP signal was observed under a fluorescent microscope. Scale bar: 400µm. (B) Flow cytometry data showed most cells expressed EGFP after doxycycline induction.

Upon establishment of doxycycline-inducible Cas9-EGFP parent cell lines, these cells were subsequently transfected with non-targeting sgRNA (**nt**), sgRNA^{ms1} (**ms1**), and sgRNA^{ms2} (**ms2**) individually to establish sgRNA-expressing cell lines. Clonal cell lines were established after selection with hygromycin. A total of two cell lines for each sgRNA were established and used for subsequent experiments. RT-PCR results showed constitutive sgRNA expression across all individual cell lines (Figure 17).
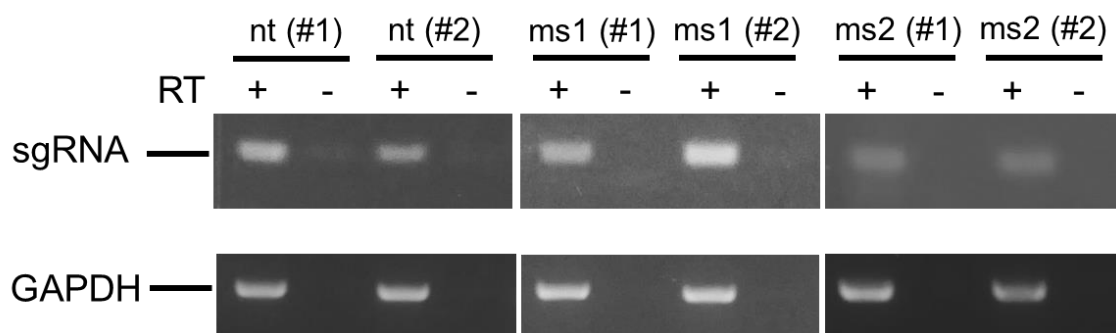
Figure 17. Expression of sgRNA and GAPDH in each individual HEK293T cell line using RT-PCR. RT: reverse transcriptase.

Cells were then treated with doxycycline for 72 hours and examined for various cellular changes and defects, such as DNA DSB using γH2AX staining, apoptotic status by annexin V

35

and propidium iodide (PI) staining, and cell proliferation ability using MTT assay and BrdU staining.

3.3.1   DNA DSB analysis

The occurrence of DNA double-strand break (DSB) in cells triggers histone H2AX phosphorylation at serine 139, also known as γH2AX, at the sites of DNA damage[47]. The presence of γH2AX is one of the earliest responses to DNA DSB, and thus can be used as a molecular marker for the detection of DNA DSBs[84]. Since sgRNA[ms] recognize multiple sites in the genome, it was hypothesized that Cas9-sgRNA[ms] cleavage activity can cause high levels of DNA damage and γH2AX foci formation, which is detectable via immunostaining.

Doxycycline treatment was conducted on inducible Cas9-EGFP and sgRNA[ms]-expressing HEK293T for 72 hours and cells were stained with anti-γH2AX (Figure 18A). Cell morphology examination showed that multinucleated cells (yellow arrowhead) and flattened cells (white arrowhead) were observed under bright field imaging (Figure 18A). The γH2AX intensity of a minimum of 50 EGFP$^+$ cells in each cell line was measured and analyzed using ImageJ software. Results showed a significant increase in γH2AX level upon Cas9-sgRNA[ms] expression (Figure 18B), suggesting that designed sgRNA[ms] were able to induce high levels of DNA DSB in HEK293T cells.
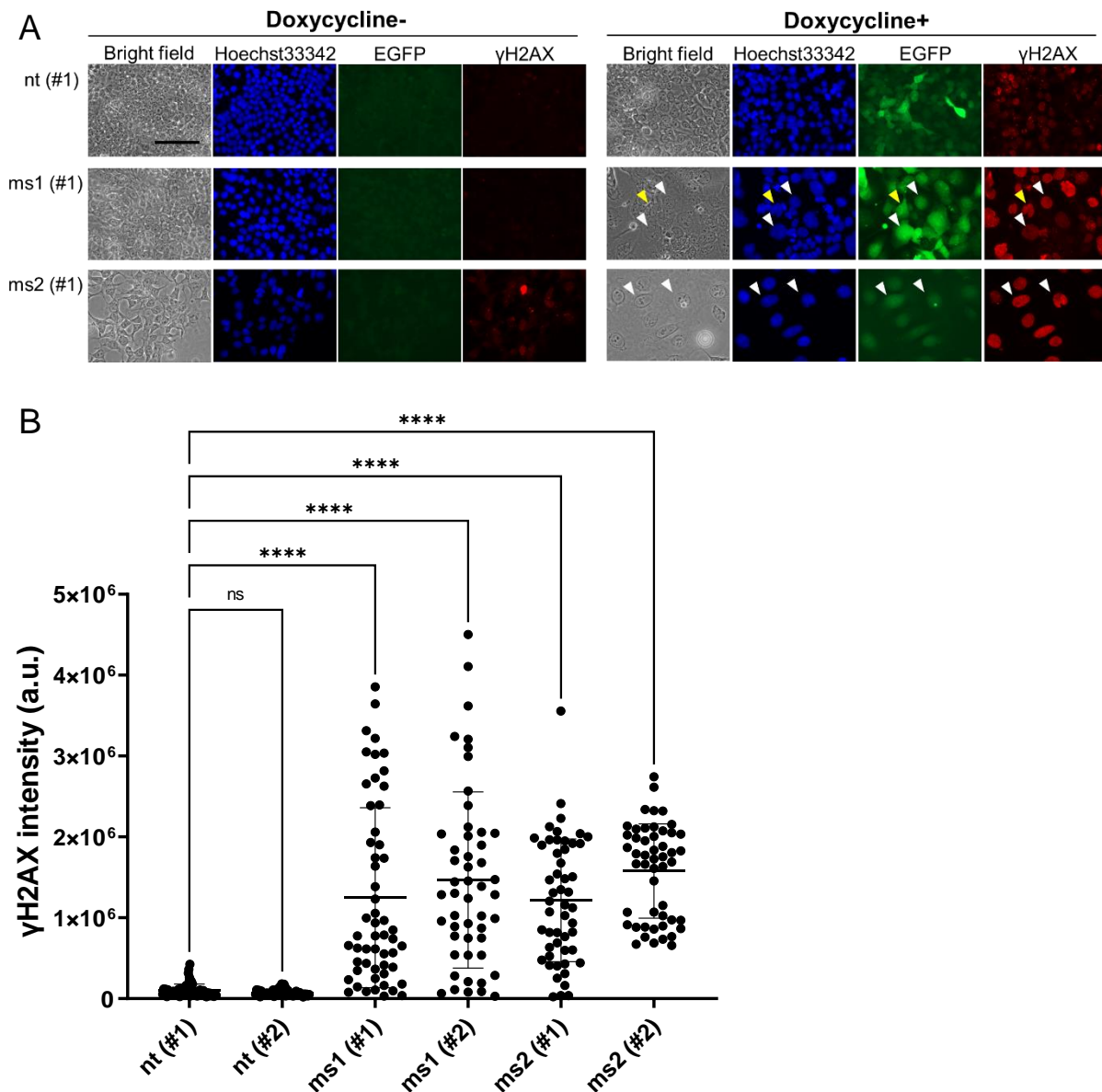
Figure 18. Increase in γH2AX signal in the presence of Cas9-sgRNA^ms expression using HEK293T cell lines. (A) Immunostaining results of γH2AX (red) in the absence and presence of doxycycline (Cas9 expression) and sgRNA^ms. Doxycycline-induced cell lines showed flattened cell morphology (white arrowhead) and multiple-nucleated cells (yellow arrowhead). Scale bar: 100µm. (B) Graph showing the intensity of γH2AX among EGFP+ cells across different genotypes. a.u.: arbitrary unit. Mean ± S.D. Statistical analysis: One-way ANOVA, ****$p<0.0001$.

3.3.2 Cell apoptosis status analysis

To further understand if the cells are undergoing cell death after 72 hours of Cas9-EGFP expression, cells were harvested and stained with annexin V and PI, followed by flow cytometry analysis. EGFP+ cells were gated and assessed for PI+ and annexin V+ cell populations. Results showed that ms1 and ms2 cell lines showed a general trend of increase in apoptotic populations (Figure 19). In both ms1 and ms2 cell lines, there was an increase in both early and late apoptotic cells, suggesting the Cas9-sgRNA^ms system was able to induce low

37

levels of cell death. Since only a small proportion of early and late apoptotic cells was detected, other cellular defects caused by the Cas9-sgRNA^{ms} system were investigated.
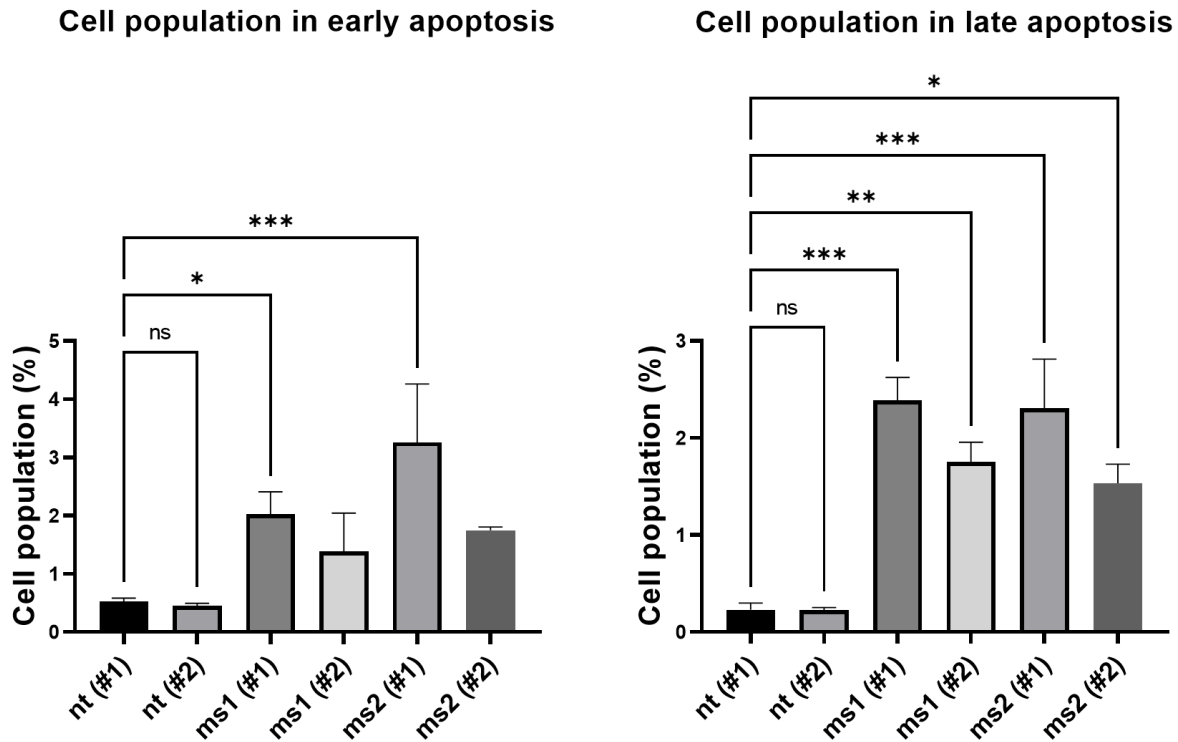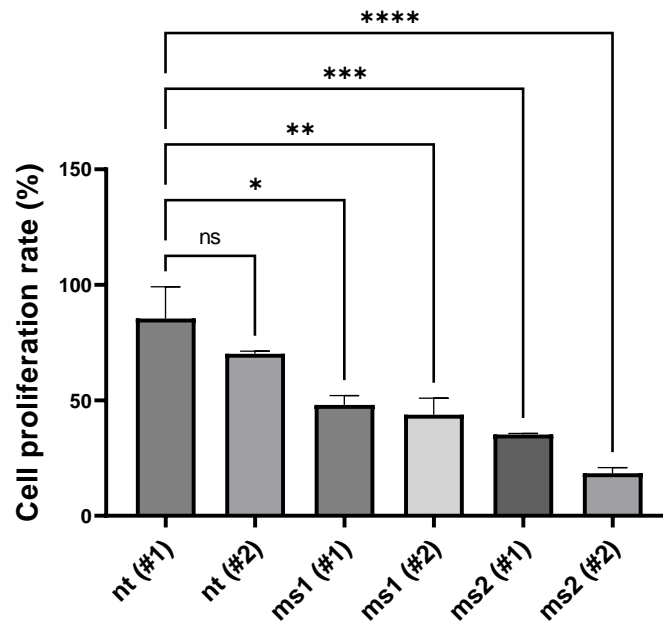

Figure 19. Cell lines expressing sgRNA^{ms1} and sgRNA^{ms2} showed an increase in early and late apoptosis cell population after 72 hours of doxycycline induced-expression of Cas9-EGFP. Mean ± S.D. Statistical analysis: One-way ANOVA. $*p<0.05$, $**p<0.01$, $***p<0.001$, $****p<0.0001$. ns: no significance.

3.3.3 MTT assay

To examine the cell viability after induction of Cas9-EGFP in the presence or absence of sgRNA^{ms}, an MTT assay was conducted. The MTT (3-(4,5-dimethylthiazol-2-yl)-2,5-diphenyltetrazolium bromide) tetrazolium was added to cultured cells in a 96-well plate. Metabolically active, viable cells convert MTT into insoluble, purple-colored formazan products. The reduction of MTT substrate was carried out by transferring an electron from the NADH molecule, reducing MTT into formazan. It was known that the quantity of formazan produced is directly proportional to the viable cell number and absorbance of formazan can be measured after solubilization. Thus, the MTT assay serves as a method to gauge the amount of metabolically active, viable cells[85]. After 72 hours of doxycycline induction, cells were treated with MTT for 3 hours, and formazan formed was solubilized. A_{595} was measured using a plate reader. The cell proliferation rate (%) was calculated using the formula below.

$$Cell\ proliferation\ rate\ (\%) = \frac{A595nm\ Dox + ve}{A595nm\ Dox - ve} \times 100\%$$

The cell proliferation rate of individual cell lines before and after doxycycline induction was calculated and compared across all cell lines. Results of the MTT assay showed that there was a significant decrease in cell proliferation in the presence of sgRNA^{ms1} or sgRNA^{ms2}, compared to the sgRNA^{nt} cell lines (Figure 20). This data suggests that cells expressing sgRNA^{ms} were still able to proliferate upon Cas9 expression, but they were proliferating at a slower rate.


Figure 20. HEK293T cell lines expressing sgRNA^{ms1} and sgRNA^{ms2} showed a decrease in cell survival rate after 72 hours of doxycycline-induced Cas9-EGFP expression. Mean ± S.D. Statistical test: One-way ANOVA. n=3. *$p<0.05$; **$p<0.01$; ***$p<0.001$; ****$p<0.0001$. ns: no significance.

3.3.4 DNA synthesis assay

To determine if cell proliferation was slower or completely inhibited upon Cas9-sgRNA^{ms} expression, BrdU immunostaining was performed. A thymidine analogue of 5-bromo-2'-deoxyuridine (BrdU) was used during cell culture. Actively proliferating cells incorporate BrdU into newly synthesized DNA during the S-phase of the cell cycle and can be easily detected through immunostaining[86]. To assess DNA synthesis, Cas9-EGFP was firstly induced for 48 hours, then BrdU was added and further incubated for another 24 hours. Cells were then harvested to determine BrdU incorporation. Results showed that most of the cells expressing non-targeting sgRNA were BrdU-positive while BrdU-negative cells were detected in cells expressing sgRNA^{ms1} and sgRNA^{ms2}. Furthermore, these BrdU-negative cells were also presented with multiple nuclei and flattened cell morphology (Figure 21A). A minimum of 100 cells in each condition were examined for the presence or absence of BrdU incorporation. Results showed that there was a significant difference in the percentage of BrdU-negative cells in ms1 and ms2 cell lines after doxycycline induction (Figure 21B). This data corroborates with

MTT assay results, suggesting that the Cas9-sgRNA^ms system inhibited cell proliferation in a portion of the cells.
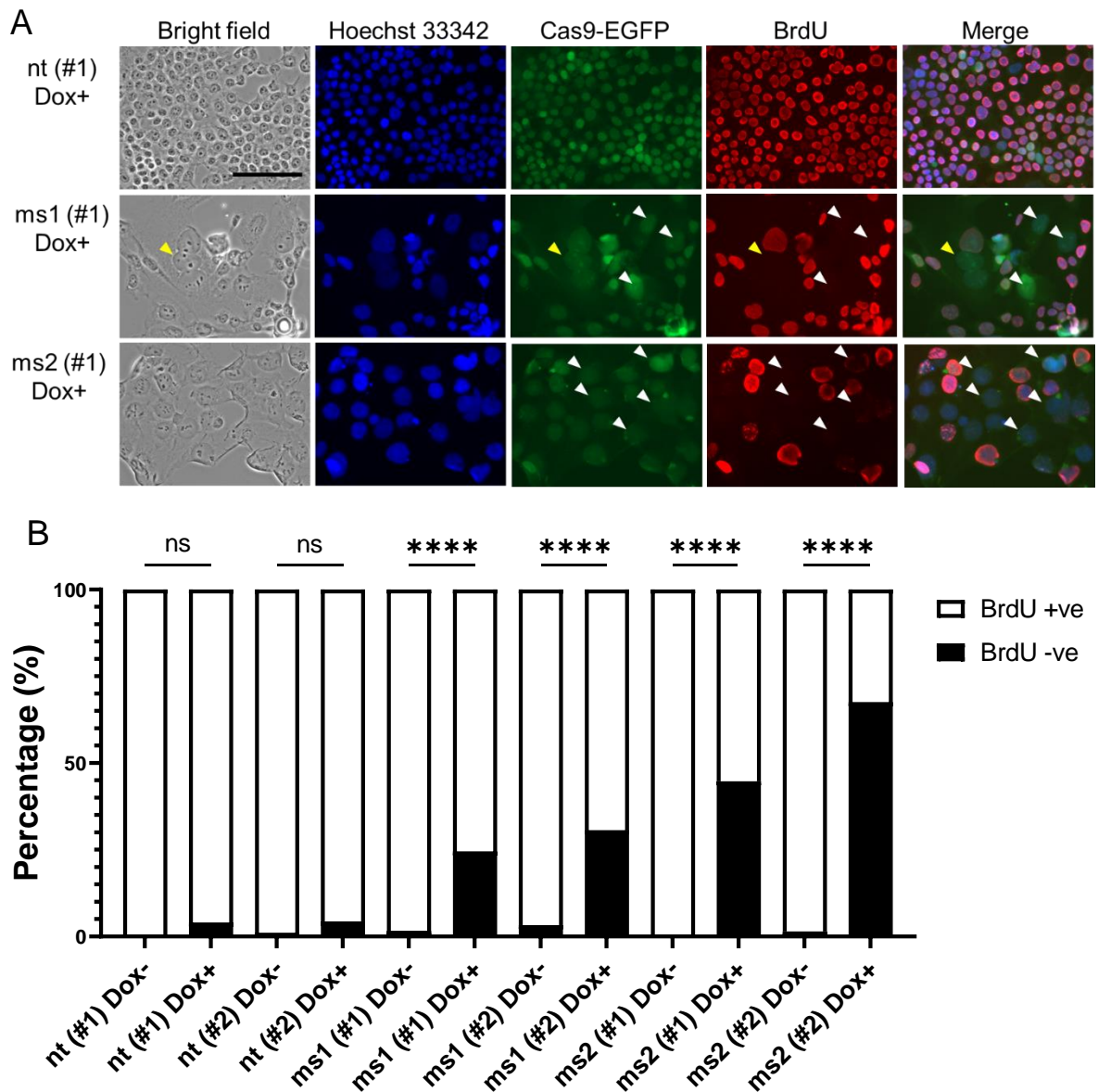
Figure 21. DNA proliferation assay showed an increase in cell number with inhibited cell proliferation ability. (A) BrdU immunostaining after doxycycline induction showed cells with no BrdU staining presented with multiple nuclei (yellow arrowhead) and flattened morphology (white arrowhead). Blue: Hoechst33342; Green: Cas9-T2A-EGFP; Red: BrdU. Scale bar: 100µm. (B) Significant increase in BrdU-negative cells upon Cas9-sgRNA^ms expression. Statistical analysis: Fischer's exact test. *$p<0.05$; ****$p<0.0001$. ns: no significance.

3.4   Validation of Cas9-sgRNA^ms function in mESCs

Since the purpose of the designed sgRNA^ms is to generate organ-deficient mouse models, thus it is important to investigate the function of Cas9-sgRNA^ms in the context of the mouse genome using mESCs. If cells transfected with Cas9-sgRNA^ms can survive, this suggests that sgRNA^ms did not successfully induce cell death upon multiple site DNA DSB.

Cells without transfection were used as a negative control, whereas cells transfected with only Cas9-expressing plasmid with no sgRNA^{ms} were used as a positive control. Results from three individual experiments showed that the number of colonies was significantly lower than positive control in the presence of sgRNA^{ms1} and sgRNA^{ms2} (Table 18 and Figure 22).

Table 18. Number of surviving mESC colonies after transfection with sgRNAms

| Condition	Colony number*			
	Trial 1	Trial 2	Trial 3	Average
No transfection	0	0	0	0
Non-targeting sgRNA (nt)	25	17	25	22.3
sgRNA^{ms1} (ms1)	4	2	4	3.3
sgRNA^{ms2} (ms2)	1	2	2	1.7

Only colonies larger than 0.1mm^2 were counted
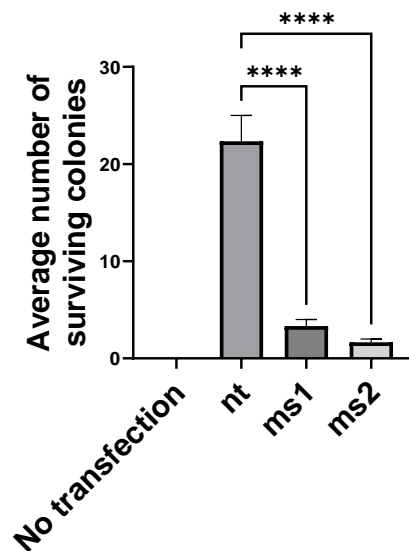
Figure 22. Average number of surviving ESC colonies under different experimental conditions. Mean ± SD. Statistical analysis: One-way ANOVA, ****$p<0.0001$.

3.5   Involvement of *p53* in Cas9-sgRNA^{ms} system

It was well known that *p53* is the tumor suppressor gene that plays a pivotal role in activating cell cycle arrest and cell death response upon DNA DSB. If knocking out *p53* in Cas9-sgRNA^{ms}-expressing mESCs decreases apoptotic cell population, then this would suggest that *p53* plays a role in Cas9-sgRNA^{ms}-induced cell death. Two sgRNA were used to knock out the *p53* gene with Cas9 to generate *p53$^{-/-}$* mESCs. RT-PCR was conducted to determine *p53* and *EpCAM* (mESCs marker) expression. Results showed that generated *p53$^{-/-}$* cell lines lack *p53* mRNA expression (Figure 23). Cell lines with normal karyotypes were used in this experiment.
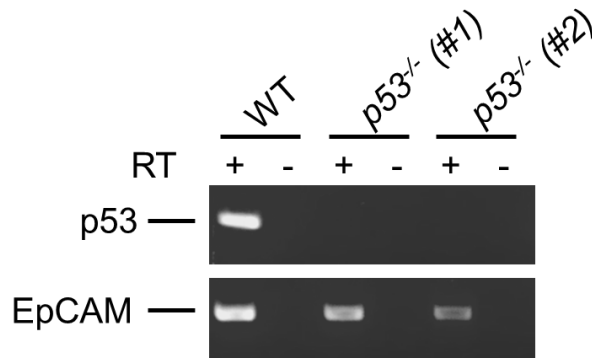
Figure 23. RT-PCR of *p53* and *EpCAM* in two *p53*⁻ᐟ⁻ mESC lines. RT: reverse transcriptase; WT: wild type.

Plasmids expressing Cas9-T2A-EGFP under the control of Cbh promoter, with or without sgRNA^{ms} were transfected to 5×10^4 mESCs and flow cytometry analysis was carried out 72 hours post-transfection. AxV and PI staining was carried out to determine cell population in the early or late apoptosis stage. Successfully transfected cells express EGFP and are gated to determine cell populations in the early and late apoptosis stage. FACS analysis results showed that wild-type mESCs transfected with Cas9-sgRNA^{ms1} and Cas9-sgRNA^{ms2} had a significant increase in the early and late apoptosis cell population. In *p53*⁻ᐟ⁻ mESCs, there was a significant decrease in the early apoptotic population compared to wild-type mESCs transfected with Cas9-sgRNA^{ms1} and Cas9-sgRNA^{ms2} (Figure 24. However, a significant decrease in the late apoptotic population was only observed in *p53*⁻ᐟ⁻ mESCs transfected with Cas-sgRNA^{ms2} (Figure 24). Taken all together, these data suggest that the designed sgRNA^{ms} were able to cause cell death in a *p53*-dependent manner.
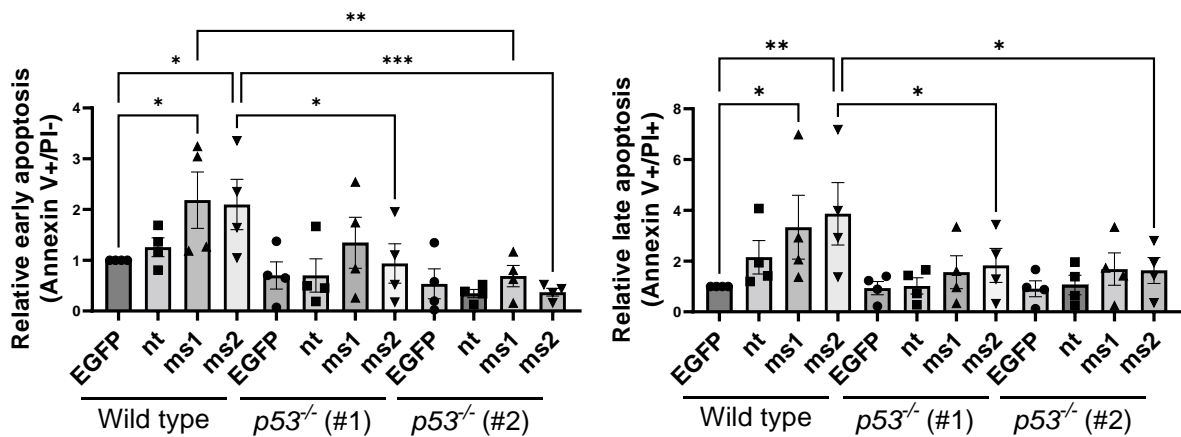

Figure 24. Increase in relative cell population in early apoptosis and late apoptosis 72 hours after transfection with Cas9-sgRNA^{ms}-expressing plasmids on wild type and *p53*⁻ᐟ⁻ mESCs. Mean ± SEM. Statistical analysis: One-way ANOVA, $*p<0.05$, $**p<0.01$, $***p<0.001$.

3.6   *In vitro* validation of *Rosa26_ms(pT-)* function

To allow constitutive expression of sgRNA[ms] in mESCs, human U6 promoter-sgRNA[ms] sequences were knocked-in at intron 1 of *Rosa26*, using CpfI protein (Figure 10). Cell lines *Rosa_ms1(pT-)* and *Rosa_ms2(pT-)* were generated. Genotype through PCR confirmed the correct knock-in sequence and karyotyped for normal chromosome count. After establishing these cell lines, Cas9-expressing plasmids were transfected to investigate the function of sgRNA[ms]. PX459 (Cas9-T2A-Puro[R] expressing-plasmid) was transfected to these cell lines to observe the cell death phenomenon, compared to the negative control without transfection and mock transfection of the pCAG-tdTomato-T2A-Puro[R] plasmid. After puromycin selection for 3 days, mESCs were stained with ALP and purplish-pink coloration indicated surviving ESCs.

The mESCs transfected with Cas9 showed almost no surviving cells when compared to the cells in the mock condition (Figure 25). This suggests that *Rosa26_ms(pT-)* cell lines were expressing functional sgRNA[ms] and were able to induce cell death upon Cas9 expression.
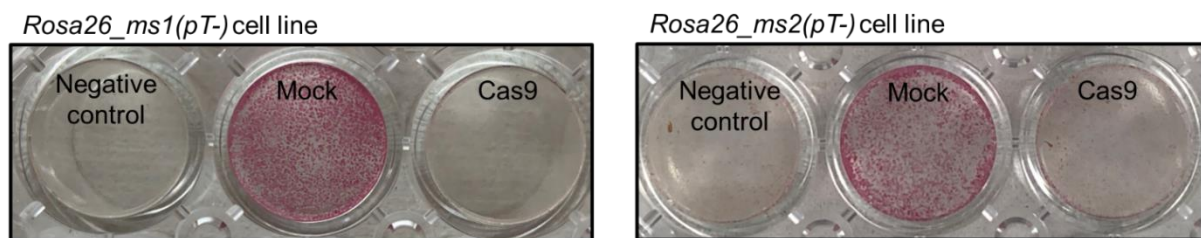
Figure 25. Cell lines transfected with Cas9 showed almost no surviving mESCs. Negative control: Non-transfected cells; Mock: pCAG-tdTomato-T2A-Puro[R] transfection; Cas9: PX459 transfection.

Since sgRNA[ms1] and sgRNA[ms2] have a different number of targeting sites in the mouse genome, it is interesting to investigate if the number of sites correlates to the efficiency of causing cell death *in vitro* after DNA DSB. Using *Rosa26_ms(pT-)* mESCs, cells transfected with pCAG-Cas9-T2A-Puro[R] were compared to cells transfected with pCAG-tdTomato-T2A-Puro[R] as transfection efficiency control. After 3 days of puromycin selection, mESCs in each condition were stained with stem cell marker, SSEA1, to quantitate the number of surviving cells. By comparing the number of SSEA1^{+} cells in both transfections using flow cytometry, the number of cells predicted to have undergone cell death caused by Cas9-sgRNA[ms] was calculated.

Data showed that Cas9-sgRNA[ms1] and Cas9-sgRNA[ms2] were able to induce cell death up to 94.89% and 59.04%, respectively in mESCs. Data showed that predicted cell death in mESCs expressing Cas9-sgRNA[ms2] was significantly lower compared to that of Cas9-sgRNA[ms1] (Figure 26). The lower rate of cell death induced by Cas9-sgRNA[ms2] could be due to lesser target sites throughout the mouse genome (Table 6).
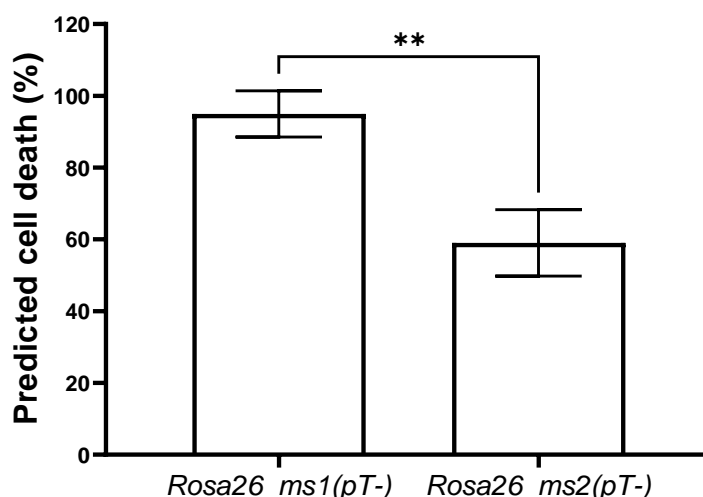
Figure 26. Predicted cell death caused by individual sgRNA^{ms} in mESCs. Mean ± S.D. Statistical analysis: Student's *t*-test, **$p<0.05$.

Chimeric mice were generated from these cell lines (Table 19) and germline transmission was confirmed from F1 generation pups after backcrossing with C57BL6/J adult female mice.

**Table 19. Summary of established *Rosa26_ms(pT-)* cell lines and chimeric pups**

Cell line	Number of pups	Number of chimeric pups	Percentage of chimeric pups (%)
#1-3 *Rosa26_ms1(pT-)*	13	13	100.00
#6-3 *Rosa26_ms1(pT-)*	10	9	90.00
#2-2 *Rosa26_ms2(pT-)*	16	15	93.75

3.7 *Foxn1* expression pattern analysis

Before establishing Cas9-expressing mESC lines under the control of the organ-specific promoter, the *Foxn1* gene expression pattern was first verified to confirm its expression in the thymus. Since *Foxn1* was known to be expressed in TECs[87], the reporter line of *Foxn1*$^{EGFP/+}$ was established using EGR-101 mESCs. Genotyping and karyotyping were before establishing chimeric mice.

The generated chimeras were dissected at E11.5 and E13.5 to examine the EGFP expression pattern in the embryos. At E11.5 and E13.5, the chimerism was determined from the appearance of black-colored eyes contributed by the EGR-101 mESC line, in contrast to white-colored eyes developed from ICR embryos.

Results showed E11.5 *Foxn1*$^{EGFP/+}$ chimeric embryo in comparison to wild-type littermate (Figure 27). Upon inspection of the whole embryo, green fluorescence was seen, specifically at the third pharyngeal pouch (white arrow).
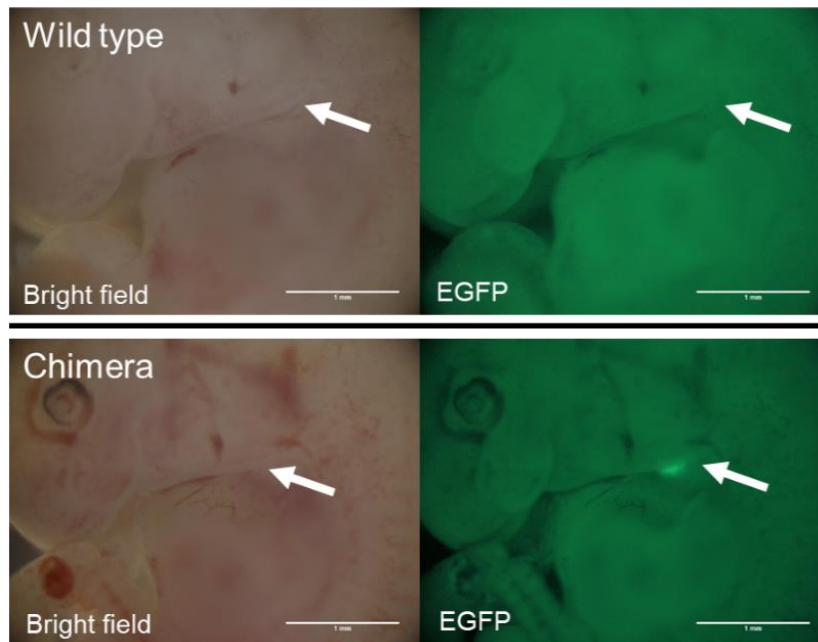
Figure 27. *Foxn1*$^{EGFP/+}$ chimeric embryo. Wild type (top panel) and *Foxn1*^{EGFP} chimera (bottom panel) of E11.5 embryos with EGFP signal at third pharyngeal pouch (white arrows). n=14 (chimera). Scale bar: 1mm.

Subsequently, E13.5 chimeric embryos were dissected, and all organs were investigated for the expression of EGFP. A strong EGFP signal was detected only from the thymus at E13.5 (Figure 28). This corroborated the data of specific expression of *Foxn1* in the developing primordial thymus[64,65].
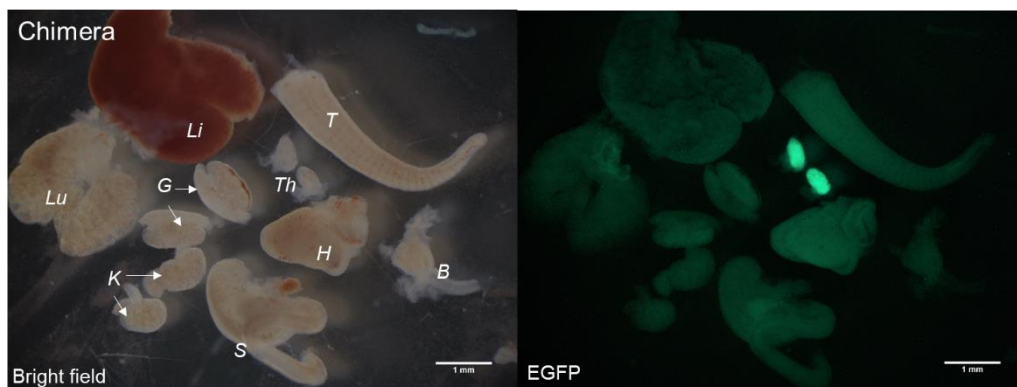
Figure 28. Organs of *Foxn1*$^{EGFP/+}$ chimeric embryo. Dissected chimeric embryo at E13.5 showed strong EGFP expression in the thymus. Li: Liver; T: Tail; Lu: Lungs; G: Gonads; Th: Thymus; H: Heart; B: Bladder; K: Kidney; S: Stomach and intestine. n=19 (chimera). Scale bar: 1mm.

Next-generation pups of *Foxn1*^{EGFP} on post-natal day (P)9 were dissected and checked for EGFP expression in the thymus. EGFP expression was detectable at this stage, indicating that *Foxn1* was expressed (Figure 29). No EGFP expression on other body parts was detected under the fluorescence microscope.
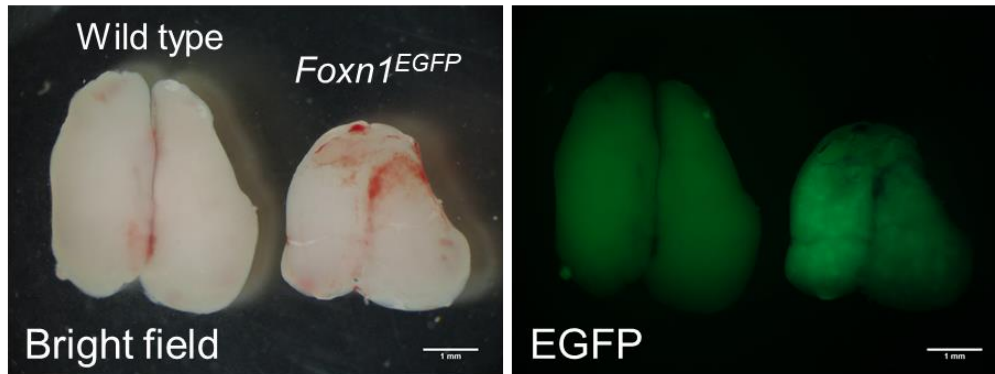
Figure 29. The thymus in the *Foxn1*^{EGFP/+} chimeric mouse. P9 thymus of wild type (left) compared to *Foxn1*^{EGFP} thymus (right) analyzed for EGFP expression under fluorescent microscope. n=3. Scale bar: 1mm.

P14 *Foxn1*^{EGFP} thymus was fixed and sectioned to examine for EGFP expression patterns in different compartments of the thymus. Thymus sections were stained with anti-GFP antibody to better visualize EGFP expression. Results showed that EGFP expression was patchy across the thymus, but an anti-GFP antibody was able to detect low levels of EGFP expression using immunostaining (Figure 30).
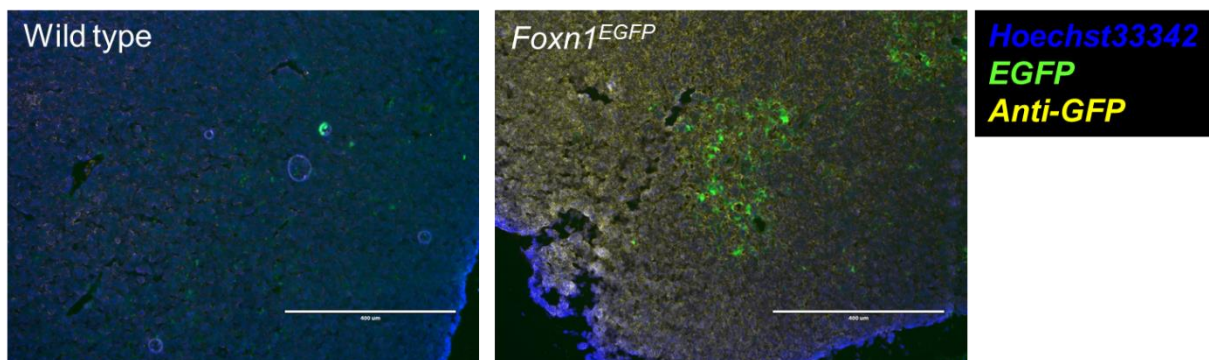
Figure 30. P14 *Foxn1*^{EGFP} thymus section stained with anti-GFP antibody. Blue: Hoechst33342; Green: EGFP; Yellow: Anti-GFP antibody. Scale bar: 400μm.

3.8 Establishment of *Foxn1*^{Cas9};*Rosa26_ms(pT-)* mouse lines

Thus far, it has been shown that Cas9-sgRNA^{ms} caused several types of cellular defects such as cell death induction and cell proliferation inhibition in HEK293T and mESCs. *Foxn1*^{EGFP} chimera has also shown specific expression of the *Foxn1* gene in the mouse thymus. Therefore, to use this novel system to generate organ-deficient mice, the thymus has been chosen to be the target organ because athymic mice have been reported to be viable[88], and is feasible to analyze the function of the Cas9-sgRNA^{ms} system in generating organ-deficient mouse model at different stages of the mouse development.

For the *in vivo* studies, cell lines *Rosa26_ms1(pT-)* and *Rosa26_ms2(pT-)* were used to conduct knock-in of Cas9 cDNA at *Foxn1* exon 2 (similar to *Foxn1^{EGFP}*) using CpfI protein. This generates cell lines with double knock-in, *Foxn1^{Cas9};Rosa26_ms(pT-)*. These cells were injected into 8-cell stage mouse embryos to establish chimeric mouse lines (Table 20).

Table 20. Generated chimeric mouse lines of *Foxn1^{Cas9};Rosa26_ms(pT-)*

Established mESC lines	Genotype		Number of pups	Number of chimeric pups	Percentage of chimeric pups (%)
	Foxn1	**Rosa26**			
#10-4	▲/Cas9	ms1/ms1(pT-)	12	10	83.30
#4-3	Cas9/Cas9	ms1/ms1(pT-)	21	16	76.20
#1-8	WT/Cas9	ms2/ms2(pT-)	5	2	40.00
#9-2	Cas9/Cas9	ms2/ms2(pT-)	8	8	100.00

Remarks: Foxn1-▲ *indicates 5bp deletion in the* Foxn1 *allele.*

3.9   Analysis of Cas9-sgRNAms system *in vivo*

The generated chimeric mice of *Foxn1^{Cas9};Rosa26_ms(pT-)* were mated to obtain next generation pups. F1 generation mice were dissected at age P9 to determine the presence or absence of thymus. Results showed that the thymus was present, and the ratio of thymus weight (mg) to body weight (g) of each mouse was computed and compared across different genotypes. Representative thymus from different genotypes was presented (Figure 31). Although complete thymus-deficiency was not observed in *Foxn1^{Cas9};Rosa26_ms(pT-)* mice, thymus to body weight ratio showed a decrease in thymus size compared to the wild type and control (lacking Cas9 and/or sgRNA^{ms} of Cas9-sgRNA^{ms} system) thymus (Figure 32).

Age	Postnatal day 9			
Genotype	WT	*Foxn1^{Cas9}; Rosa26_ms1(pT-)*	*Foxn1^{Cas9}; Rosa26_ms2(pT-)*	*Foxn1^{Cas9}; Rosa26_ms1/ms2(pT-)*
Thymus (mg) to body weight (g) ratio	4.7818	2.7925	2.8036	2.1132
Thymus photograph				

Figure 31. Thymus to body weight ratio data and thymus phenotype observation from mice with different genotypes

Since sgRNA^{ms1} and sgRNA^{ms2} did not cross-recognize (Figure 13B), thus, to increase the number of DNA DSB in TEC, mice with both sgRNA^{ms}, *Foxn1^{Cas9};Rosa26_ms1(pT-)/ms2(pT-)*, were generated and examined. However, results showed that the relative thymus size was similar to that of *Foxn1^{Cas9};Rosa26_ms(pT-)* and was not significantly reduced (Figure 32).
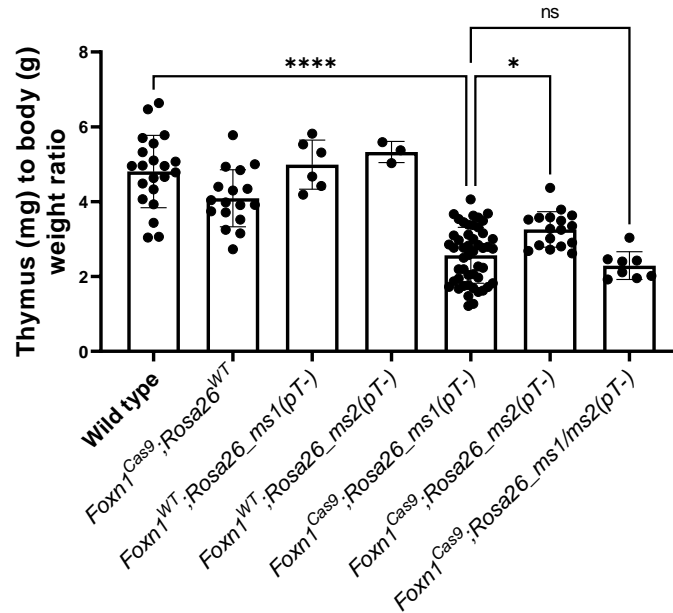
Figure 32. Thymus (mg) to body (g) weight ratio across mice of different genotypes at P9. Mean ± S.D. Statistical analysis: One-way ANOVA, *$p < 0.05$, ****$p < 0.0001$, ns: no significance.

To confirm the expression of Cas9 and sgRNA^{ms}, RNA was extracted from the thymus of *Foxn1^{Cas9};Rosa26_ms1(pT-)* pups at P9. Reverse transcription was conducted, and the cDNA product was used for RT-PCR analysis. Results showed that expression of Cas9 and sgRNA^{ms1} mRNA was detected across all three pups (Figure 33).
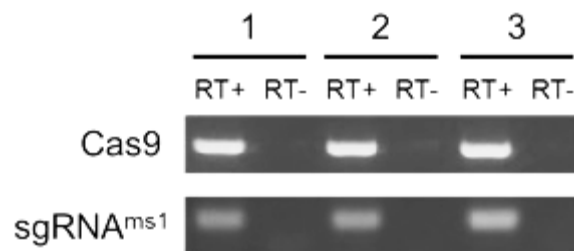
Figure 33. RT-PCR from thymus of three different *Foxn1^{Cas9};Rosa26_ms1(pT-)* pups at P9. RT: reverse transcriptase.

Since results showed that increasing the number of target sites did not further reduce thymus size, thus it was hypothesized that increasing the Cas9 amount could induce more DNA DSB, and further cause thymus shrinkage or complete thymus ablation. To increase the Cas9 amount, extra copies of Cas9 cDNA were knocked-in under the *Foxn1* promoter. *Foxn1^{Cas9-}*

$^{T2A-Cas9}$;*Rosa26_ms1* was generated from *Foxn1^{Cas9};Rosa26_ms1(pT-)* by knocking in T2A-Cas9 cassette downstream of *Foxn1^{Cas9}*, and *Foxn1-3'UTR^{Cas9};Rosa26_ms1(pT-)* (homozygous Cas9) was generated from *Rosa26_ms1(pT-)* mESCs. Homozygous *Foxn1-3'UTR^{Cas9}* mouse would produce FOXN1-T2A-Cas9 protein since Cas9 was knocked in downstream of the *Foxn1* coding sequence, at the start of 3'UTR. To further increase Cas9, *Foxn1-3'UTR^{Cas9}* mice were crossed with *Foxn1$^{Cas9-T2A-Cas9}$* mice, producing *Foxn1$^{Cas9-T2A-Cas9}$;Foxn1-3'UTR^{Cas9}* mice with 3 copies of Cas9 cDNA, while the retaining expression of FOXN1 protein (Figure 34). Next generation mice with different genotypes and Cas9 cDNA copy numbers were analyzed at P9 to examine the thymus phenotype.
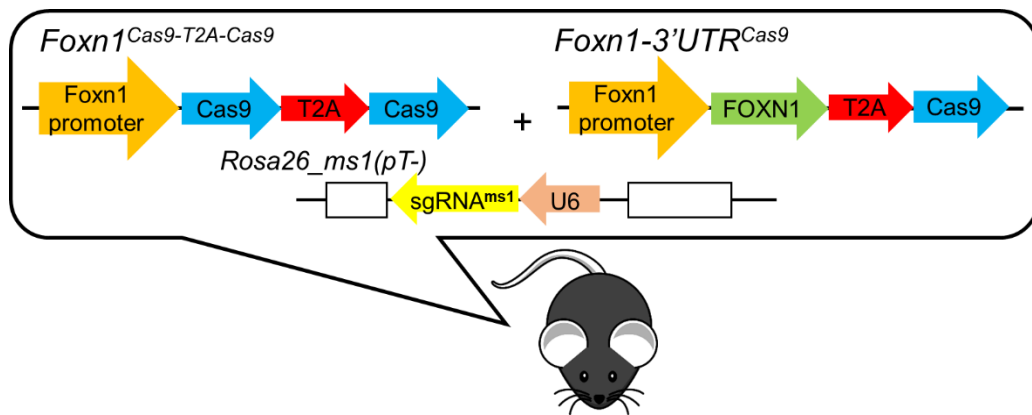
Figure 34. Schematic diagram showing *Foxn1$^{Cas9-T2A-Cas9}$;Foxn1-3'UTR^{Cas9}* mouse model with 3 copies of Cas9 cDNA under *Foxn1* promoter

Results showed that the relative size of the thymus with more copies of Cas9 cDNA did not significantly decrease compared to *Foxn1^{Cas9};Rosa26_ms(pT-)*, and there was no significant difference compared to that of the control group (Figure 35).
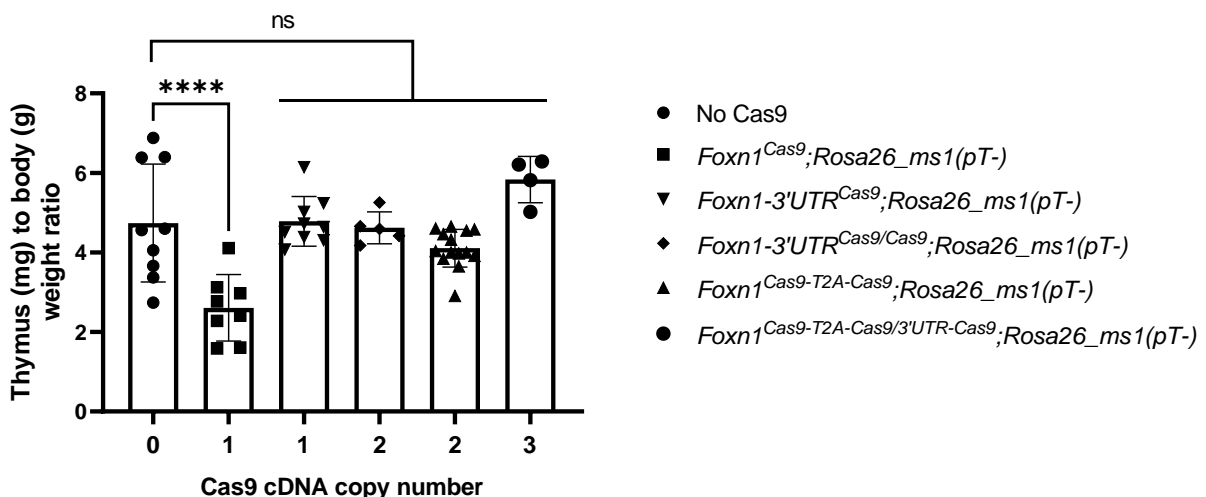
Figure 35. Results of relative thymus size in mice with different Cas9 copy number. Mean ± S.D. Statistical analysis: One-way ANOVA, ****$p<0.0001$, ns: no significance.

To verify Cas9 expression in the thymus, RNA and whole protein lysate were collected from the P9 thymus of mice with an alternative Cas9 expression cassette. RT-PCR was conducted with EpCAM (thymic epithelial cell marker) as an internal control. The intensities of RT-PCR bands were quantified using ImageJ and Cas9 band intensity relative to EpCAM band intensity was calculated. Results showed no difference in Cas9 mRNA expression in the thymus across different genotypes (Figure 36). This implied that although Cas9 mRNA was being expressed, only $Foxn1^{Cas9};Rosa26\_ms1(pT\text{-})$ mice showed a decrease in thymus size, further suggesting that Cas9 protein might not be translated or defective in $Foxn1\text{-}3'UTR^{Cas9}$ and $Foxn1^{Cas9\text{-}T2A\text{-}Cas9}$ mice.
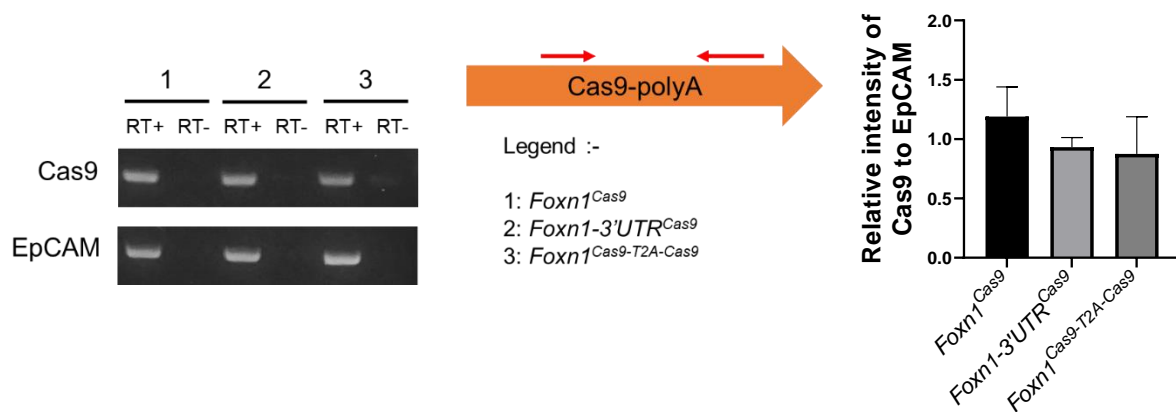
Figure 36. RT-PCR analysis of P9 thymus of different genotypes to determine Cas9 expression level. RT: reverse transcriptase.

To determine Cas9 expression at the protein level, western blot analysis was conducted. Anti-Cas9 and anti-EpCAM antibodies were used to determine protein expression. Results showed that Cas9 was expressed in mouse thymus of all different genotypes, with EpCAM as an internal control (Figure 37A). Relative band intensity of Cas9 to EpCAM was quantified and found that $Foxn1^{Cas9}$ and $Foxn1\text{-}3'UTR^{Cas9}$ have similar Cas9 protein expression, while $Foxn1^{Cas9\text{-}T2A\text{-}Cas9}$ showed relatively lower Cas9 expression (Figure 37B).
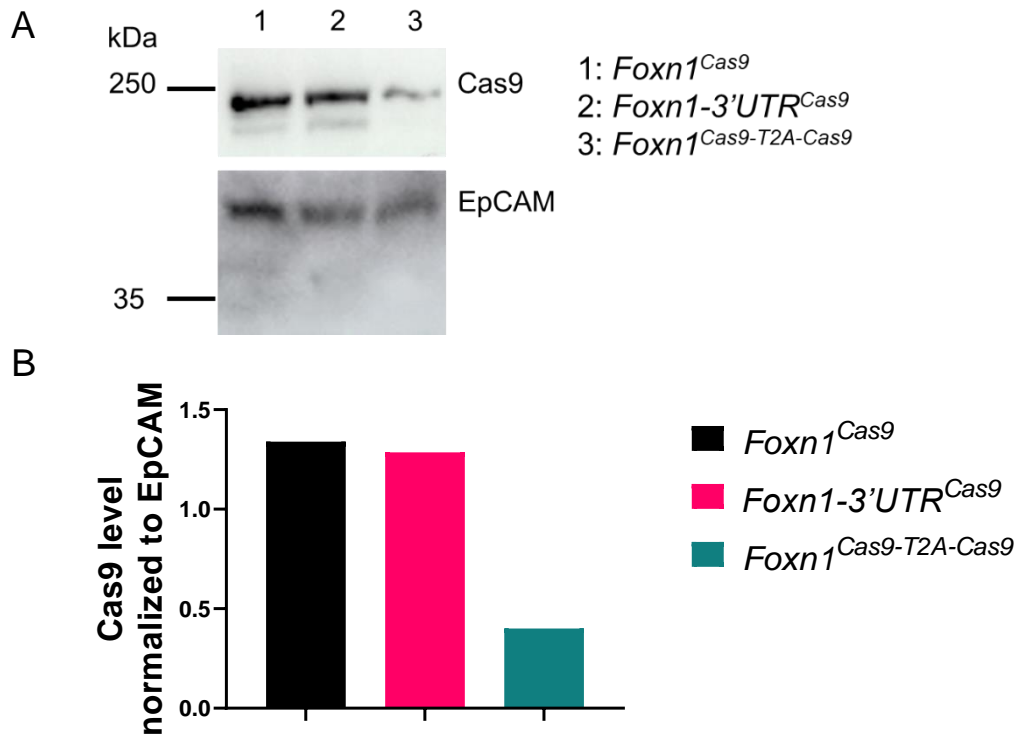
Figure 37. Western blot analysis to determine Cas9 expression in thymus under *Foxn1* promoter in mice with different constructs. (A) Western blot analysis of whole protein lysate from the thymus. (B) Relative expression of Cas9 to EpCAM in the thymus.

3.10 Microscopic analyses of *Foxn1*^{Cas9}*;Rosa26_ms1(pT-)* thymus

It was reported that thymus involution or atrophy occurs in mice starting at around two months old and thymus size starts decreasing[89]. Thymus involution is also associated with the breakdown of thymus architecture, whereby the cortex and medulla are no longer clearly demarcated[90]. Thus, the morphology and function of *Foxn1*^{Cas9}*;Rosa26_ms1(pT-)* small thymi were further analyzed.

H&E staining was conducted on the P9 thymus section to investigate for any morphological changes in thymic architecture. The tissue section showed clear demarcation of corticomedullary junction (CMJ) in both control and *Foxn1*^{Cas9}*;Rosa26_ms1(pT-)* thymi (Figure 38). There were no obvious architectural differences between the two thymi. These thymi were also stained with cortex and medulla-specific markers, K8 and K5, respectively, to further identify the tissues present. Results showed that the cortex and medulla were clearly identified with the correct structure and location in the thymus (Figure 39). No observable difference was detected from H&E staining and immunostaining results of *Foxn1*^{Cas9}*;Rosa26_ms1(pT-)* thymus compared to control.
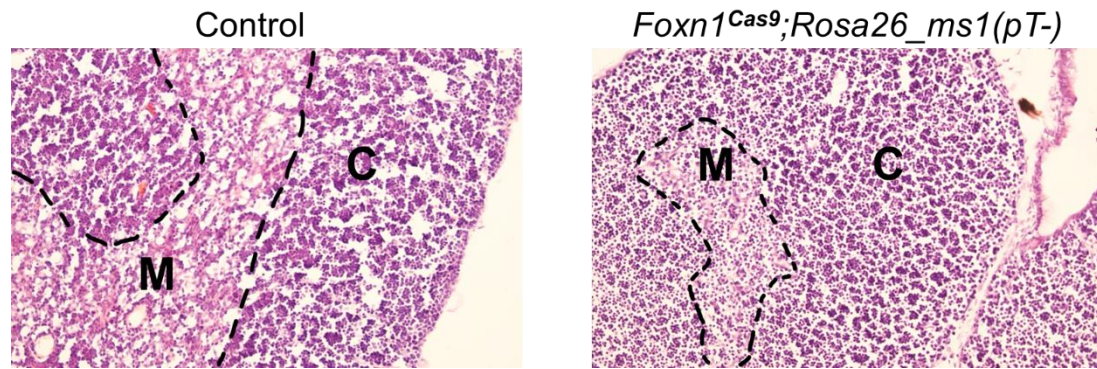
Figure 38. H&E staining of P9 thymus. Control thymus (left) compared to *Foxn1^{Cas9};Rosa26_ms1(pT-)* thymus (right). The CMJ is marked by black dotted lines. C: Cortex; M: Medulla. Magnification: 200x.
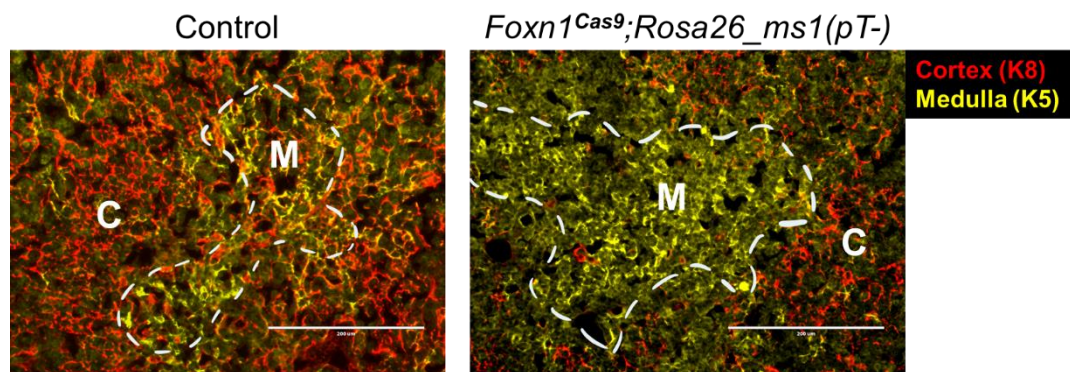
Figure 39. Immunostaining of P9 thymus sections. The thymus sections were stained with anti-K8 (red) and anti-K5 (yellow) antibodies, specifying the cortex and medulla, respectively. Control thymus (left) compared to *Foxn1^{Cas9};Rosa26_ms1(pT-)* thymus (right). Scale bar: 200µm.

3.11 Analysis of thymus function

The small thymus is one of the signs of thymic involution, which is usually present in aged mice and humans. This alters the efficiency and population of thymocytes produced in the thymus[90]. One of the main functions of the thymus is that it serves as the site for T cell education and maturation. The incoming immature thymopoiesis-initiating progenitors from the bone marrow interact with the thymic epithelial cells[91]. Thymocytes then undergo positive selection to mature into $CD45^+/CD3^+$ T cells with $CD8^+$ or $CD4^+$ in the thymus cortex, followed by negative selection in the thymus medulla[92]. The mature T cells then migrate out from the thymus into the peripheral circulation and accumulate in the spleen, a secondary lymphoid organ[93,94].

To examine thymus function, the spleen and thymus were harvested from P9 and P90 mice and investigated for the cell population present using flow cytometry. Splenocytes and thymocytes were stained with α-CD45 (lymphocytes), α-CD3 (T cells), α-CD4 (T_H cells), and α-CD8 (T_C cells). The ratio of T cells among lymphocytes ($CD3^+/CD45^+$) was first computed.

Further T cell subpopulations were calculated as a percentage of CD4 and CD8 double positive (CD4$^+$;CD8$^+$) immature T cells, CD4 single positive (CD4$^+$;CD8$^-$) T$_H$ cells, and CD8 single positive (CD4$^-$;CD8$^+$) T$_C$ cells, among total CD3$^+$ T cells.

Results of P9 mice showed that there was a significant decrease in T cell ratio in the thymus and spleen of *Foxn1^{Cas9}-Rosa26_ms1(pT-)* mice compared to that of control. However, the T cell ratio of *Foxn1^{Cas9}-Rosa26_ms2(pT-)* mice only affected the spleen (Figure 40A, B). T cell ratio in thymus and spleen was affected only in *Foxn1^{Cas9}-Rosa26_ms1(pT-)* P90 mice, but not *Foxn1^{Cas9}-Rosa26_ms2(pT-)* (Figure 40C, D).
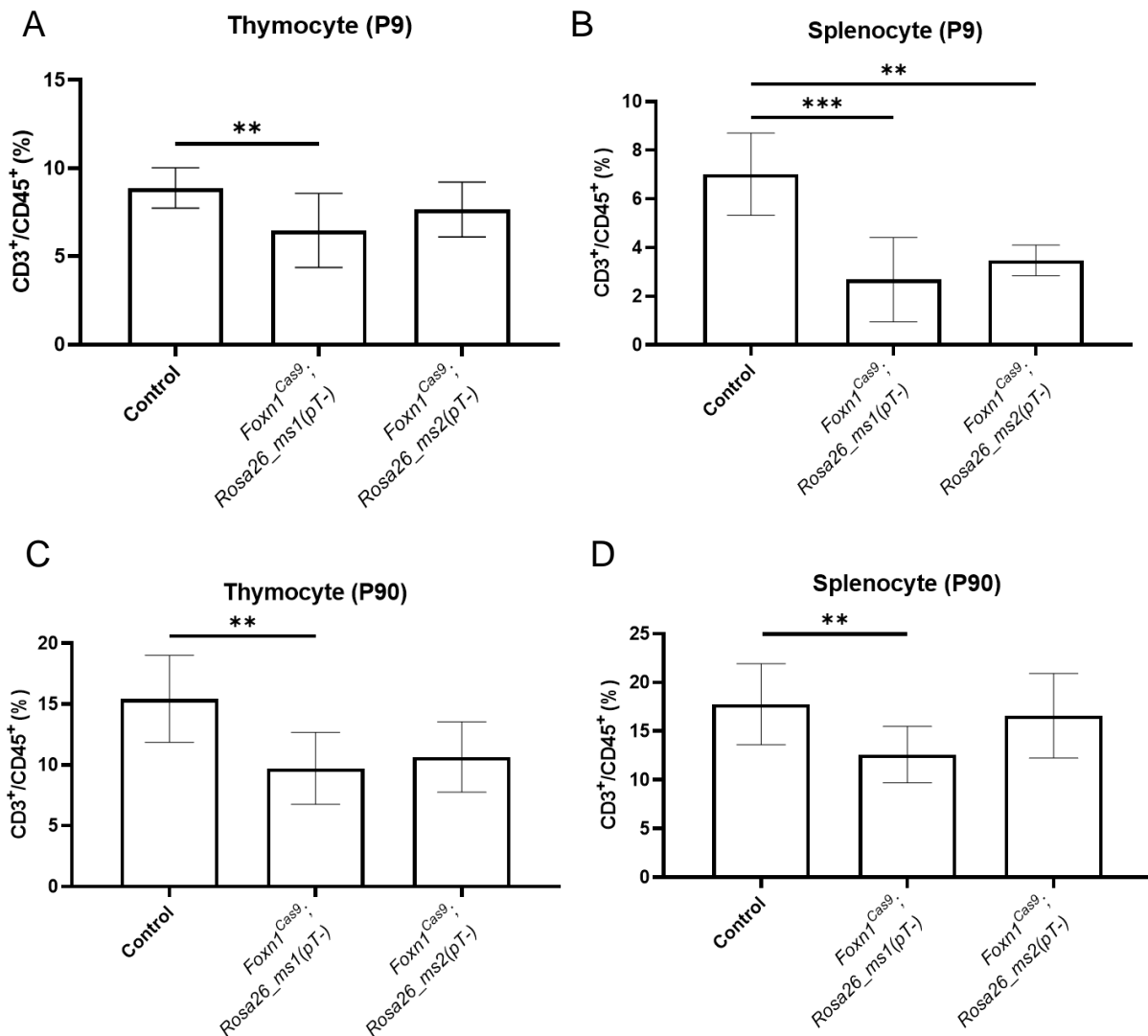
Figure 40. Ratio of T cells among lymphocytes at different age. Samples of P9 thymocyte (A) and splenocyte (B), and P90 thymocyte (C) and splenocyte (D). Mean ± S.D. Statistical analysis: Student's *t*-test, **$p<0.01$, ***$p<0.001$.

CD3$^+$ T cells were further analyzed for different subpopulations. Data showed that there was no significant difference in these T cell subpopulations across all groups of mice at P9 (Figure 41A, B) and P90 (Figure 41C, D).
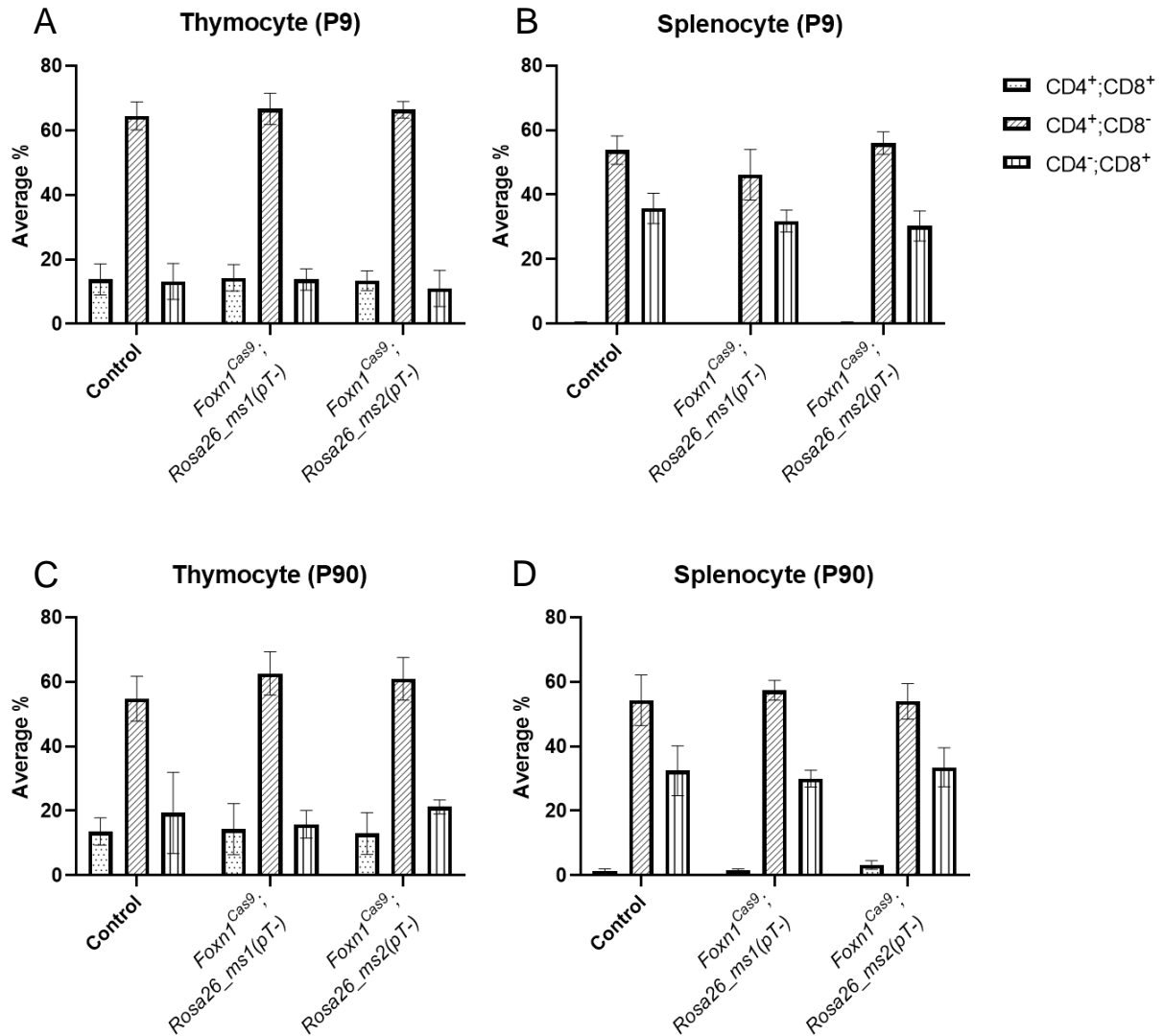
Figure 41. T cell subpopulations at different age. T cell subpopulations in P9 thymocyte (A) and splenocyte (B), and P90 thymocyte (C) and splenocyte (D). All results showed no significant difference compared to the control group. Mean ± S.D. Statistical analysis: One-way ANOVA.

Since this Cas9-sgRNA^{ms} system could induce high levels of DNA DSB and possibly generate high levels of indel mutation, there is a possibility for the TECs of *Foxn1^{Cas9};Rosa26_ms(pT-)* mice to develop into cancer. Therefore, adult mice at age P90 were dissected to observe if the small thymus phenotype persist and if there are any morphology of cancer. Results of the thymus to body weight ratio showed that there was no significant difference in *Foxn1^{Cas9};Rosa26_ms(pT-)* mice compared to the control group (Figure 42).
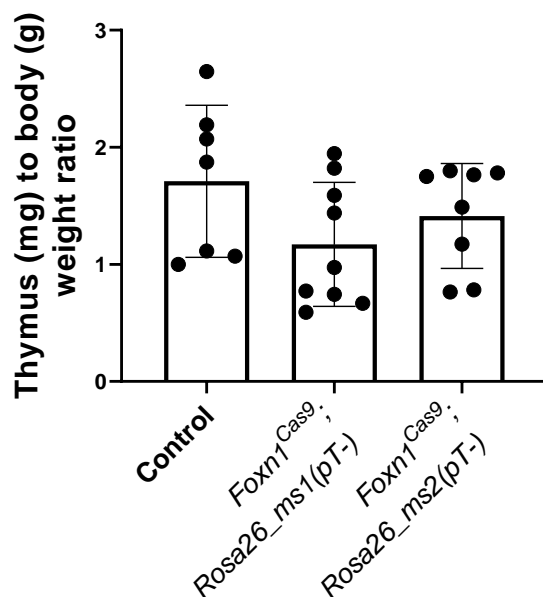
Figure 42. Thymus (mg) to body (g) weight ratio across mice of different genotypes at P90. No significant difference in thymus to body weight ratio was observed across all mice. Mean ± S.D. Statistical analysis: One-way ANOVA.

3.12   Improvement of Cas9-sgRNA^{ms} system

It was reported that a longer poly-T tail of 6bp to 10bp appended to the downstream of sgRNA scaffold showed higher sgRNA termination efficiency[95], thus a poly-T tail of 6bp was added to sgRNA^{ms} construct and knocked in at *Rosa26* locus to generate mESCs. Table 21 showed established *Rosa26_ms* cell lines and generated chimeric founder mouse.

Table 21. Summary of established *Rosa26_ms* cell lines and chimeric pups

mESC line	Number of pups	Number of chimeric pups	% of chimeric pups
Rosa26_ms1	12	12	100.0%
Rosa26_ms2	7	7	82.4%

To test if these established mESC lines can induce cell death upon Cas9 expression, a Cas9-expressing plasmid with puromycin resistance gene was transfected and selected with puromycin. ALP staining results showed that there was a minimal amount of surviving mESCs (Figure 43), suggesting cell death was successfully induced in *Rosa26_ms* cell lines.
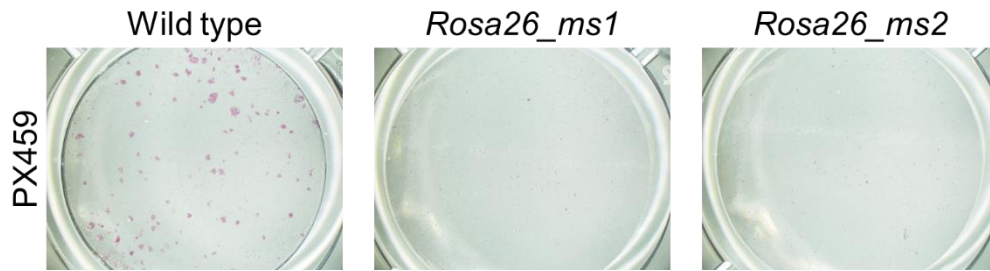
Figure 43. Minimal amount of surviving cell (purplish-pink coloration) after Cas9-expression in *Rosa26_ms1* and *Rosa26_ms2* cell lines

Chimeric founder mice of *Rosa26_ms1* and *Rosa26_ms2* were established and crossed with *Foxn1^{Cas9}* mice to generate *Foxn1^{Cas9};Rosa26_ms*, which are hypothesized to become thymus-deficient mouse models. Next generation pups were examined at P9 for the presence or absence of thymus. Results showed that thymus was absent in all examined *Foxn1^{Cas9};Rosa26_ms* pups, whereas thymus was present in control mice (mice lacking Cas9-sgRNA^{ms} system) (Figure 44).
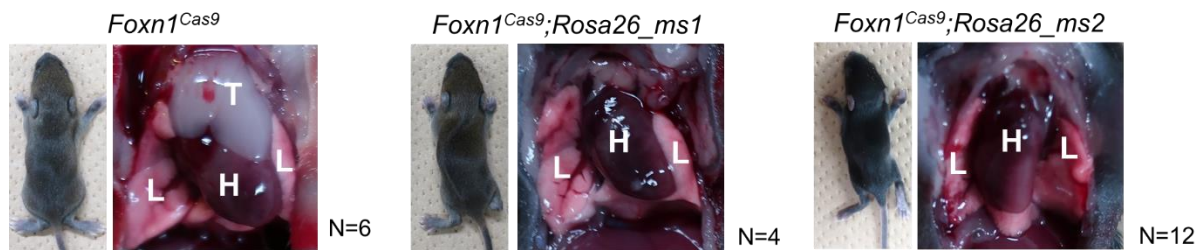
Figure 44: Athymic phenotype in *Foxn1^{Cas9};Rosa26_ms* mice. T: thymus; L: lungs; H:heart.

To confirm the athymic phenotype, splenocytes were harvested and determined for the presence of CD3$^+$/CD45$^+$ peripheral T cells using flow cytometry analysis. Results showed that only a minimal CD3$^+$/CD45$^+$ T cell population was detected in the athymic mice compared to control mice (Figure 45), suggesting the lack of functional thymus in *Foxn1^{Cas9};Rosa26_ms* mice.
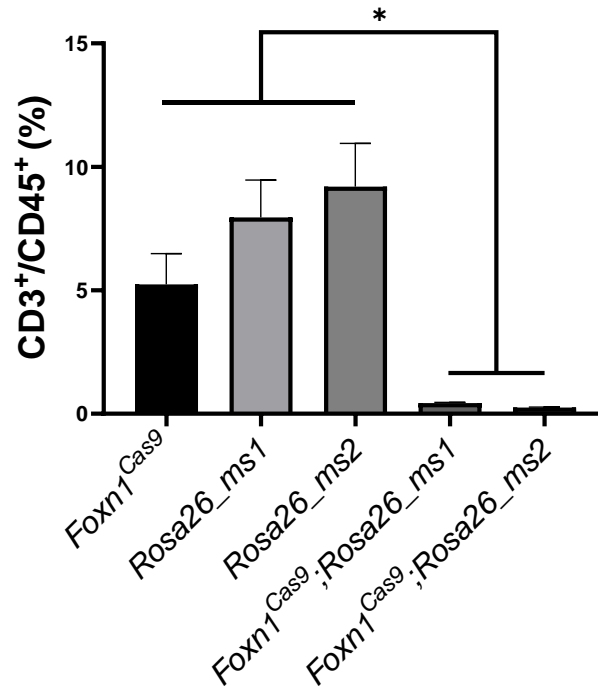
Figure 45. Flow cytometry analysis of CD3$^+$ T cells among CD45$^+$ lymphocytes in the spleen of P9 mice across different genotypes

.

3.13 Generation of rat thymus in *Foxn1^{Cas9};Rosa26_ms.pT* mouse ← rat chimera

The goal of generating organ-deficient mouse models is to overcome organ shortage by producing organs from injected PSCs, through interspecies blastocyst complementation. Since sgRNA^{ms2} has lesser target sites compared to sgRNA^{ms1}, sgRNA^{ms2} theoretically would cause lesser DNA DSB in the genome. Thus, only sgRNA^{ms2} was used for subsequent blastocyst complementation experiments. To generate thymus from rat origin, rat ESCs with constitutive EGFP expression were injected into *Foxn1^{Cas9};Rosa26_ms2* blastocyst at E2.5. These embryos were transferred to pseudopregnant mice to complete the gestational period. The embryos and pups were dissected at E18.5 to determine the contribution of rat cells to the thymus.

Table 22 shows a summary of the blastocyst complementation experiments conducted to generate mouse←rat xenogeneic chimera.

Table 22. Summary of xenogeneic chimera experiments

Analysis age	Embryos injected	No. of embryos	No. of chimeric embryos	Target genotype (*Foxn1^{Cas9};Rosa26_ms2*)
E18.5	106	35	11	4

The gross morphology of E18.5 complemented thymus from *Foxn1^{Cas9};Rosa26_ms2* host embryos showed strong EGFP expression compared to the control host embryos (Figure 46A). Similarly, the thymus section in the control host showed a partial contribution of rat ESC-derived thymic cells while *Foxn1^{Cas9};Rosa26_ms2* host generated thymus with rat ESC-derived thymic cells throughout almost the entire section (Figure 46B).
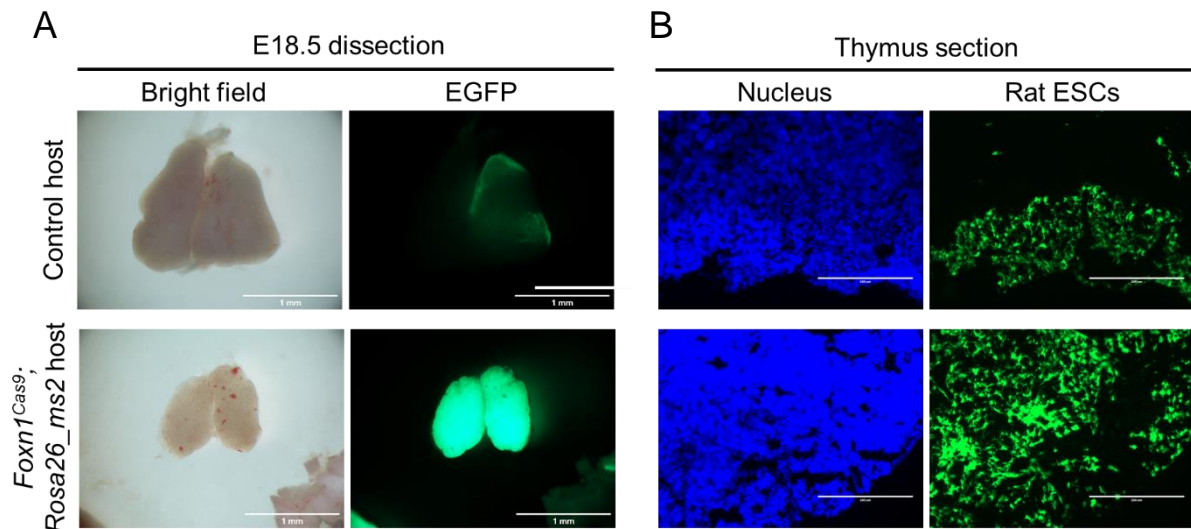
Figure 46: Dissection of E18.5 xenogeneic chimera to determine rat cell contribution in the thymus. (A) Gross morphology of E18.5 xenogeneic thymus. Green: Rat ESC-derived cells. Scale bar: 1mm. (B) Section of E18.5 xenogeneic thymus. Green: Rat ESC-derived cells. Scale bar: 200µm.

To understand the extent of the contribution from rESC to the thymus, these thymi were sectioned and subjected to immunostaining. Cytokeratin 8 (K8) and cytokeratin 5 (K5) are epithelial cell markers of the cortex and medulla region, respectively. The anti-K8 antibody only recognizes mouse cTECs while the anti-K5 antibody cross-recognizes both mouse and rat mTECs.

In *Foxn1^{Cas9};Rosa26_ms2* host, EGFP signal was detected almost uniformly across the cross-section of the complemented thymus (Figure 47). Furthermore, there was almost no overlapping region between rat-derived cells and the mouse cortex region in the control thymus, suggesting that the contribution of rESCs was limited when host-derived cells are present. In *Foxn1^{Cas9};Rosa26_ms2* host embryos, there were no mouse cTECs detected. This suggests that most of the thymic epithelial cells were derived from the injected rat ESCs.
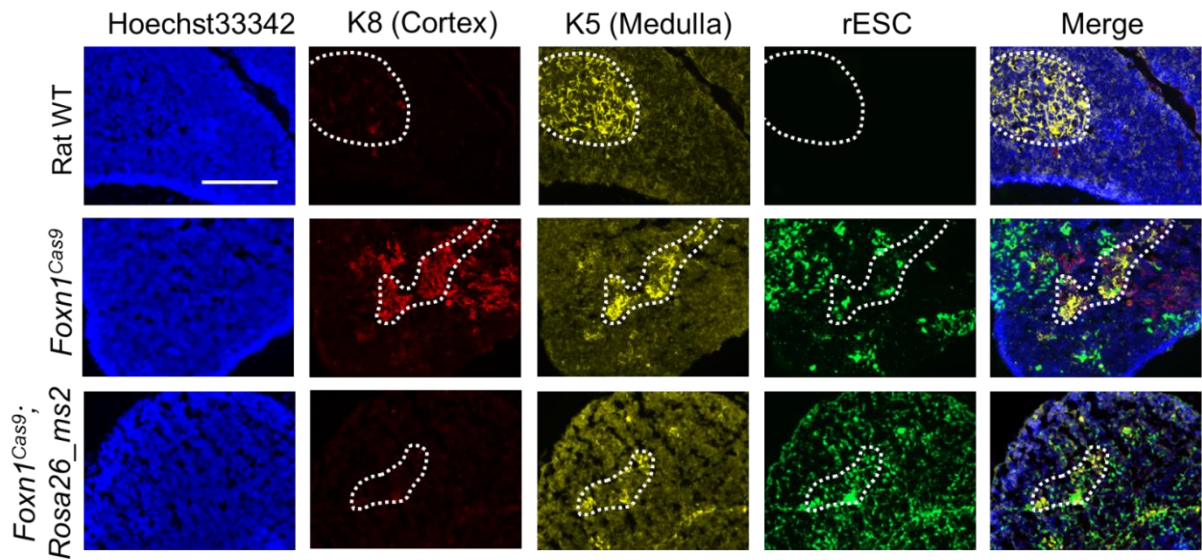
Figure 47. Contribution of rat cells (green) in thymus of wild-type rat and xenogeneic chimera host of *Foxn1^Cas9* and *Foxn1^Cas9;Rosa26_ms2*, stained with anti-K8 (red) and anti-K5 (yellow) antibody. Dotted line marks medulla region. Scale bar: 200µm

Chapter 4 – Discussion

In this study, the main idea is to engineer a new method to generate an organ-deficient mouse model via CRISPR-Cas9 technology by designing sgRNA[ms] that recognize multiple sites throughout the genome in several species. Through the designed Cas9-sgRNA[ms] system, it was hypothesized that cellular defects can be induced, eventually causing cell ablation in an organ-specific manner when Cas9 is expressed in organ-specific progenitor cells. This method aims to improve efficiency in producing organ-deficient mouse blastocysts. By complementing organ-deficient blastocyst with stem cells from a different target species, the organ of interest can be procured for transplantation. This would provide an alternative solution to overcome the problem of organ shortage.

4.1 Cellular defects and athymic phenotype caused by Cas9-sgRNA[ms] system

Combining *in vitro* and *in vivo* data, the designed Cas9-sgRNA[ms] system induced cell ablation through DNA DSB induction, cell apoptosis, and cell proliferation defects, which eventually led to the complete ablation of the thymus. Based on the inducible Cas9-EGFP HEK293T cell line experiment, it was shown that expression of Cas9-sgRNA[ms] generated high levels of γH2AX and significantly increased the percentage of BrdU-negative cells. These data suggested that the Cas9-sgRNA[ms] system successfully induced the accumulation of DNA DSB and decreased cell proliferation.

Furthermore, almost all ms1 and ms2 cells showed whole-cell nucleus γH2AX staining and multiple γH2AX foci after Cas9 expression (Figure 18A). The current study also showed the presence of multinucleated cells, flattened cell morphology, and enlarged nucleus after induction of Cas9 in sgRNA[ms]-expressing HEK293T cell lines (Figure 18A), suggesting cell senescence. Although *in vitro* data showed only a low percentage of apoptotic cells after Cas9 expression, the possibility of Cas9-sgRNA[ms] inducing more cell death or cell clearance at a later stage has yet to be clarified. Phagocytes have been reported to be able to engulf senescent cells[96,97], and apoptotic cells[98,99] at different stages through accumulation and release of different signals.

It was reported that cells with irreparable DNA damage trigger either programmed cell death or cellular senescent to prevent cell progression[100]. The multiple DNA DSB in cells has been reported to trigger cell cycle arrest through the *p53-p21* pathway[101]. Previous reports found that flattened and multinucleated cells are classical phenotypes of senescent cells[101]. These reports corroborate with current data suggesting that Cas9-sgRNA[ms] could trigger cellular defects such as apoptosis and senescence. However, the presence of key senescent markers such as the senescence-associated-beta-galactosidase (SA-β-gal) activity and senescence-associated secretory phenotype (SASP) have to be further examined[100].

Reports also suggested that cellular senescence can be induced by prolonged and mild DNA damage while apoptosis can be activated by acute DNA damage[100,102,103]. The current *in*

vitro doxycycline-induced Cas9-EGFP study was only conducted for a short period while Cas9-expression under *Foxn1* occurs over a longer period (expression from E11.5 to P9, approximately 18 days). The detailed mechanism of either cellular senescent or apoptosis triggered by Cas9-sgRNA^{ms} in the context of thymic epithelial cells has yet to be examined. Further experiments to examine these mechanisms can be conducted by expressing Cas9-sgRNA^{ms} in primary thymic epithelial cell culture at different time points. This can elucidate the mechanism of cellular defects by Cas9-sgRNA^{ms} in a temporal- and cell-type-specific context.

4.2   Involvement of *p53* in Cas9-sgRNA^{ms} system

Current results showed that there was a significant decrease in apoptotic cell population in *p53$^{-/-}$* mESCs with Cas9-sgRNA^{ms} (Figure 24). This suggests that Cas9-sgRNA^{ms} induced apoptosis through the *p53* pathway. Based on this result, it could also be implied that Cas9-sgRNA^{ms} might not work in triggering cell death of cancer cells if the *p53* gene has been disrupted. Further experiments on *p53* KO mouse must be conducted to elucidate the involvement of this pathway *in vivo*.

4.3   sgRNA^{ms} expression and termination efficiency with poly-T tail

The thymus phenotype was drastically different between mice expressing sgRNA without and with poly-T tail (*Rosa26_ms(pT-) vs. Rosa26_ms*). *Foxn1^{Cas9};Rosa26_ms(pT-)* mice generated a small thymus (Figure 31) while *Foxn1^{Cas9};Rosa26_ms* mice generated athymic mice (Figure 44). This suggests that cell ablation induced in the thymus of *Foxn1^{Cas9};Rosa26_ms(pT-)* was incomplete and only the organ size was affected. It was reported that if there are less than 6 bases of poly-T sequence downstream of sgRNA, the termination efficiency of sgRNA during transcription was significantly decreased[95]. This could suggest that in the current study, the sgRNA^{ms} produced were not successfully terminated *in vivo* and led to decreased efficiency in inducing DNA DSB in the thymic epithelial cells. Upon improving the Cas9-sgRNA^{ms} system by appending poly-T tail downstream of sgRNA^{ms}, a complete thymus-deficient mouse model was generated. This further suggests that the successfully terminated sgRNA^{ms} were able to form a complex with Cas9 and efficiently cause multiple DNA DSB in the thymic epithelial cells.

4.4   Difference in thymus and skin phenotype

It was previously found that a single base pair deletion on the *Foxn1* gene caused frameshift mutation and produced truncated FOXN1 protein, which led to the hairless and athymic phenotype[75,76]. In the skin, *Foxn1* was also known to be expressed in developing keratinocytes and played a role in the hair follicle and skin epidermal development[104,105]. The skin of *Foxn1$^{-/-}$* adult mice was found to be in the undeveloped stage and was more ready to undergo scar-free wound healing compared to scar-forming wound healing[104,106]. Although the

hair in *Foxn1*^{-/-} mice undergoes a regular hair growth cycle[107], the hairlessness phenotype was caused by impaired keratinization of the hair shaft and thus the hairs were unable to properly penetrate the outermost layer epidermal layer of the skin[108].

In this study, *Foxn1*[Cas9]*;Rosa26_ms* mouse model showed only the thymus was affected but the hair phenotype was not affected. This could suggest that there was incomplete or partial cell ablation of the *Foxn1*-expressing keratinocytes in the skin. Since it was reported that expression of FOXN1 stimulates keratinocyte growth in the neighboring cells via paracrine mechanisms[105], thus it would be possible that even a small number of Foxn1-expressing cells remained in the skin could maintain normal growth and differentiation of hair follicles and keratinocytes. However, this hypothesis still needs to be thoroughly examined in the *Foxn1*[Cas9]*;Rosa26_ms* model.

4.5 Contribution of rat ESCs to the thymus in xenogeneic chimera

Although the generated xenogeneic thymus showed high contribution (strong EGFP signal) of rat-derived cells in *Foxn1*[Cas9]*;Rosa26_ms2* host, closer examination of gross morphology showed relatively smaller thymus size compared to that of the control. This observation was consistent with previous reports of generating rat thymus in the nude mouse model, which generated a relatively smaller thymus[7]. Furthermore, the rat thymus generated in nude mice was found to be capable of T cell education upon transplantation under kidney capsule[7].

In the E18.5 xenogeneic chimera, it was found that the entirety of the thymus section showed a lack of mouse cTECs. However, the presence or absence of mouse mTECs has yet to be confirmed (Figure 47). A study on embryonic thymus development by tracking the expression of β5t, a proteasome subunit specifically expressed in cTEC but not mTEC, showed that almost all *Aire*[+] mTECs had a history of β5t expression[109]. This suggests that thymic progenitor cells first differentiated into cTECs and then further differentiated into mTEC to form a mature thymus. Furthermore, other studies have shown that mTECs were differentiated from cells that previously expressed cTEC markers such as CD205[110] and IL7[111]. Taken together, these suggest that the K5[+] medulla detected in *Foxn1*[Cas9]*;Rosa26_ms2* thymus has a high possibility to be derived from rESCs since the mouse cTEC was not detected. Current results also showed the presence of K8[+]/K5^{+} cells in the thymus, which is commonly present in the corticomedullary junction of the thymus[112].

Thymus section results showed uniform EGFP signals throughout the entirety of the organ. However, certain regions have neither EGFP nor K5/K8 signal (Figure 47), suggesting that these regions might contain non-epithelial tissue of mouse origin. It was known that the thymic environment is highly heterogenous, consisting of both epithelial and non-epithelial stromal cells[113]. The epithelial cells are derived from endodermal lineage while the other stromal cells are from mesodermal and neural crest mesenchymal lineage[114]. Thymic epithelial cell differentiation was known to be controlled by the master regulator, *Foxn1*[87], and non-

epithelial stromal cells were derived from *Foxn1*-negative lineage[115]. Hence, *Foxn1^{Cas9};Rosa26_ms* mice were hypothesized to induce cell ablation only in thymic epithelial cells. The non-epithelial stromal cells could have very well been contributed by the host cells as these stromal cells are important for the normal development of the thymus.

4.6   Advantages of novel Cas9-sgRNA^{ms} system

In this study, Cas9 was expressed under organ-specific genes to obtain organ-deficient animal models with constitutive expression of sgRNA^{ms}. This could potentially be applied to generate animals with deficiencies in different organs and hypothesized to ablate actively proliferating progenitor cells. The sequence of sgRNA^{ms} designed in this research has many targeting sites in the genome of several species, thus can be applied to generate not only organ-deficient mouse models but also larger animal models such as pigs for the procurement of human organs.

Comparing the Cas9-sgRNA^{ms} system to the gene KO method to generate organ-deficient animal models, the efficiency has increased from one-fourth to one-half by using the Cas9-sgRNA^{ms} system. This can be achieved by crossing animals with a heterozygous Cas9 knock-in to another animal with homozygous *Rosa26_sgRNA^{ms}*.

4.7   Limitations

One of the limitations of this study is that *in vitro* assays were only conducted using cultured HEK293T and mESCs. These cells are vastly different cell types compared to the organ progenitor cells where DNA DSB was hypothesized to occur. This limits the understanding of the working mechanisms of Cas9-sgRNA^{ms} that are occurring in specific organ progenitor cells. Furthermore, although the epithelial cells in the skin and thymus both express *Foxn1*, only the thymus was completely ablated in the *Foxn1^{Cas9};Rosa26_ms* mouse model, with the skin showing no observable phenotype difference. This also suggests that the downstream response of the Cas9-sgRNA^{ms} system could be different depending on cell type. To overcome this limitation, the primary culture of organ progenitor cells or organoids can be used to express the Cas9-sgRNA^{ms} system. This method will allow the prediction of cell ablation efficiency in a cell type-specific context.

Currently, there are other systems to generate organ-deficient animals, such as expressing *Hes1* under the *Pdx1* gene promoter for pancreas-deficient pigs whereby *Hes1* functions to maintain pancreatic progenitor cells in an undifferentiated state[116]. However, the expression of *Hes1* has yet to be reported to generate other organ-deficient animals and this might indicate that this technique can only be applied in a tissue-specific manner. Another method to conduct cell death is through the chemical-induced activation of the caspase proteins[117–119]. This method is usually used to ablate cells or tissue of a specific lineage at specific time points. However, the use of this method to generate organ-deficient animals has yet to be reported. The universality of the Cas9-sgRNA^{ms} system can be investigated and could

be further compared with other reported methods to understand the efficiency in generating organ-deficient animal models.

4.8   Conclusion and future direction

In conclusion, the current Cas9-sgRNA^{ms} system provides an alternative method to induce cellular defects and ablation through DNA DSB at multiple sites in an organ-specific manner. By expressing Cas9 under different organ-specific promoters simultaneously, multiple organ-deficient animal models can potentially be produced.

Chapter 5 – Acknowledgements

First and foremost, I am profoundly grateful to Associate Professor Ayako Isotani, my research supervisor, for their wise and valuable guidance throughout the planning and execution of this research study. I would also like to thank Assistant Professor Shunsuke Yuri for the time and continuous advice provided in times of adversity. To both my research advisors, Professor Taro Kawai and Professor Akira Kurisaki, thank you for the wise suggestions provided throughout my progress and for the examination of the thesis. Furthermore, my appreciation toward Mr. Kazuaki Takahashi and Ms. Ayako Takara for helping with the animal experiments and support.

Apart from that, I would also like to extend my gratitude to all members of Isotani-lab, for supporting me throughout the experimentation period. I would also like to thank my family and all my friends in NAIST for the continuous psychological support, for without them, I would not be able to persevere through the challenging times.

Finally, I sincerely thank the Ministry of Education, Culture, Sports, Science, and Technology (MEXT), Japan, for providing me with the scholarship to fund my postgraduate education at NAIST.

Chapter 6 – References

1. Aita, K. Japan approves brain death to increase donors: will it work? *The Lancet* **374**, 1403–1404 (2009).

2. Seifi, A., Lacci, J. V. & Godoy, D. A. Incidence of brain death in the United States. *Clin Neurol Neurosurg* **195**, 105885 (2020).

3. Kaufman, M. H. & Evans, M. J. Establishment in culture of pluripotential cells from mouse embryos. *Nature* **292**, 154–156 (1981).

4. Martin, G. R. Isolation of a pluripotent cell line from early mouse embryos cultured in medium conditioned by teratocarcinoma stem cells. *Proc Natl Acad Sci U S A* **78**, 7634–7638 (1981).

5. Takahashi, K. & Yamanaka, S. Induction of Pluripotent Stem Cells from Mouse Embryonic and Adult Fibroblast Cultures by Defined Factors. *Cell* **126**, 663–676 (2006).

6. Rowe, R. G. & Daley, G. Q. Induced pluripotent stem cells in disease modelling and drug discovery. *Nature Reviews Genetics* **20**, 377–388 (2019).

7. Isotani, A., Hatayama, H., Kaseda, K., Ikawa, M. & Okabe, M. Formation of a thymus from rat ES cells in xenogeneic nude mouse↔rat ES chimeras. *Genes to Cells* **16**, 397–405 (2011).

8. Mori, M. *et al.* Generation of functional lungs via conditional blastocyst complementation using pluripotent stem cells. *Nat Med* **25**, 1691–1698 (2019).

9. Kobayashi, T. *et al.* Blastocyst complementation using Prdm14-deficient rats enables efficient germline transmission and generation of functional mouse spermatids in rats. *Nat Commun* **12**, 1–10 (2021).

10. Kobayashi, T. *et al.* Generation of rat pancreas in mouse by interspecific blastocyst injection of pluripotent stem cells. *Cell* **142**, 787–799 (2010).

11. Usui, J. I. *et al.* Generation of kidney from pluripotent stem cells via blastocyst complementation. *American Journal of Pathology* **180**, 2417–2426 (2012).

12. Behringer, R. R., Gertsenstein, M., Nagy, K. V. & Nagy, A. *Manipulating the Mouse Embryo: A Laboratory Manual*. (Cold Spring Harbor Laboratory Press, 2014).

13. Kitahara, A. *et al.* Generation of Lungs by Blastocyst Complementation in Apneumic Fgf10-Deficient Mice. *Cell Rep* **31**, 107626 (2020).

14. Palmiter, R. D. *et al.* Cell Lineage Ablation in Transgenic Mice by Cell-Specific Expression of a Toxin Gene. *Cell* **50**, 435–443 (1987).

15. Matsumura, H., Hasuwa, H., Inoue, N., Ikawa, M. & Okabe, M. Lineage-specific cell disruption in living mice by Cre-mediated expression of diphtheria toxin A chain. *Biochem Biophys Res Commun* **321**, 275–279 (2004).

16. Lem, J., Applebury, M. L., Falk, J. D., Flannery, J. G. & Simon, M. I. Tissue-specific and developmental regulation of rod opsin chimeric genes in transgenic mice. *Neuron* **6**, 201–210 (1991).

17. Collier, R. J. Understanding the mode of action of diphtheria toxin: A perspective on progress during the 20th century. *Toxicon* **39**, 1793–1803 (2001).

18. Plummer, N. W., Ungewitter, E. K., Smith, K. G., Yao, H. H. C. & Jensen, P. A new mouse line for cell ablation by diphtheria toxin subunit A controlled by a Cre-dependent FLEx switch. *Genesis* **55**, (2017).

19. Breitman, M. L. *et al.* Genetic ablation: Targeted expression of a toxin gene causes microphthalmia in transgenic mice. *Science* **238**, 1563–1565 (1987).

20. Yamaizumi, M., Mekada, E., Uchida, T. & Okada, Y. One molecule of diphtheria toxin fragment A introduced into a cell can kill the cell. *Cell* **15**, 245–250 (1978).

21. Dymecki, S. M. Flp recombinase promotes site-specific DNA recombination in embryonic stem cells and transgenic mice. *Proc Natl Acad Sci U S A* **93**, 6191–6196 (1996).

22. Ivanova, A. *et al.* In vivo genetic ablation by Cre-mediated expression of diphtheria toxin fragment A. *Genesis* **43**, 129–135 (2005).

23. Saito, M. *et al.* Diphtheria toxin receptor-mediated conditional and targeted cell ablation in transgenic mice. *Nat Biotechnol* **19**, 746–750 (2001).

24. Chapman, T. J. & Georas, S. N. Adjuvant effect of diphtheria toxin after mucosal administration in both wild type and diphtheria toxin receptor engineered mouse strains. *J Immunol Methods* **400–401**, 122–126 (2013).

25. Bao, J., Ma, H. Y., Schuster, A., Lin, Y. M. & Yan, W. Incomplete Cre-mediated excision leads to phenotypic differences between Stra8-iCre; Mov10l1lox/lox and Stra8-iCre; Mov10l1lox/Δ mice. *Genesis* **51**, 481–490 (2013).

26. Barrangou, R. *et al.* CRISPR provides acquired resistance against viruses in prokaryotes. *Science* **315**, 1709–1712 (2007).

27. Safari, F., Zare, K., Negahdaripour, M., Barekati-Mowahed, M. & Ghasemi, Y. CRISPR Cpf1 proteins: structure, function and implications for genome editing. *Cell Biosci* **9**, 1–21 (2019).

28. Jinek, M. *et al.* A programmable dual-RNA-guided DNA endonuclease in adaptive bacterial immunity. *Science* **337**, 816–821 (2012).

29. Charpentier, E., Richter, H., van der Oost, J. & White, M. F. Biogenesis pathways of RNA guides in archaeal and bacterial CRISPR-Cas adaptive immunity. *FEMS Microbiol Rev* **39**, 428–441 (2015).

30. Makarova, K. S. *et al.* An updated evolutionary classification of CRISPR–Cas systems. *Nat Rev Microbiol* **13**, 722–736 (2015).

31. Mali, P. *et al.* RNA-guided human genome engineering via Cas9. *Science* **339**, 823–826 (2013).

32. Ran, F. A. *et al.* Genome engineering using the CRISPR-Cas9 system. *Nat Protoc* **8**, 2281–2308 (2013).

33. Goto, T. *et al.* Generation of pluripotent stem cell-derived mouse kidneys in Sall1-targeted anephric rats. *Nat Commun* **10**, (2019).

34. Watanabe, M. *et al.* Anephrogenic phenotype induced by SALL1 gene knockout in pigs. *Sci Rep* **9**, (2019).

35. Nishinakamura, R. & Takasato, M. Essential roles of Sall1 in kidney development. *Kidney Int* **68**, 1948–1950 (2005).

36. Zetsche, B. *et al.* Cpf1 is a single RNA-guided endonuclease of a Class 2 CRISPR-Cas system. *Cell* **163**, 759 (2015).

37. Moon, S. B. *et al.* Highly efficient genome editing by CRISPR-Cpf1 using CRISPR RNA with a uridinylate-rich 3′-overhang. *Nat Commun* **9**, 1–11 (2018).

38. Alok, A. *et al.* The Rise of the CRISPR/Cpf1 System for Efficient Genome Editing in Plants. *Front Plant Sci* **11**, 264 (2020).

39. Kwon, T. *et al.* Precision targeting tumor cells using cancer-specific InDel mutations with CRISPR-Cas9. *Proc Natl Acad Sci U S A* **119**, (2022).

40. Głów, D. *et al.* CRISPR-to-Kill (C2K)-Employing the Bacterial Immune System to Kill Cancer Cells. *Cancers (Basel)* **13**, (2021).

41. Martinez-Lage, M. *et al.* In vivo CRISPR/Cas9 targeting of fusion oncogenes for selective elimination of cancer cells. *Nat Commun* **11**, (2020).

42. Xu, L., Yu, W., Xiao, H. & Lin, K. BIRC5 is a prognostic biomarker associated with tumor immune cell infiltration. *Sci Rep* **11**, 1–13 (2021).

43. Narimani, M., Sharifi, M. & Jalili, A. Knockout Of BIRC5 Gene By CRISPR/Cas9 Induces Apoptosis And Inhibits Cell Proliferation In Leukemic Cell Lines, HL60 And KG1. *Blood Lymphat Cancer* **9**, 53 (2019).

44. Roos, W. P. & Kaina, B. DNA damage-induced cell death: From specific DNA lesions to the DNA damage response and apoptosis. *Cancer Lett* **332**, 237–248 (2013).

45. Matsumoto, Y., Asa, A. D. D. C., Modak, C. & Shimada, M. DNA-dependent protein kinase catalytic subunit: The sensor for DNA double-strand breaks structurally and functionally related to ataxia telangiectasia mutated. *Genes* **12**, (2021).

46. Yue, X., Bai, C., Xie, D., Ma, T. & Zhou, P. DNA-PKcs: A Multi-Faceted Player in DNA Damage Response. *Front Genet* **11**, (2020).

47. Burma, S., Chen, B. P., Murphy, M., Kurimasa, A. & Chen, D. J. ATM Phosphorylates Histone H2AX in Response to DNA Double-strand Breaks. *Journal of Biological Chemistry* **276**, 42462–42467 (2001).

48. Fragkos, M., Jurvansuu, J. & Beard, P. H2AX Is Required for Cell Cycle Arrest via the p53/p21 Pathway. *Mol Cell Biol* **29**, 2828–2840 (2009).

49. Wang, H. *et al.* A Perspective on Chromosomal Double Strand Break Markers in Mammalian Cells. *Jacobs J Radiat Oncol* **1**, (2014).

50.	Lee, Y., Wang, Q., Shuryak, I., Brenner, D. J. & Turner, H. C. Development of a high-throughput γ-H2AX assay based on imaging flow cytometry. *Radiation Oncology* **14**, (2019).

51.	Giglia-Mari, G., Zotter, A. & Vermeulen, W. DNA damage response. *Cold Spring Harb Perspect Biol* **3**, 1–19 (2011).

52.	Vitale, I., Manic, G., de Maria, R., Kroemer, G. & Galluzzi, L. DNA Damage in Stem Cells. *Mol Cell* **66**, 306–319 (2017).

53.	Kragelund, B. B., Weterings, E., Hartmann-Petersen, R. & Keijzers, G. The Ku70/80 ring in Non-Homologous End-Joining: Easy to slip on, hard to remove. *Front Biosci (Landmark Ed)* **21**, 514–527 (2016).

54.	Aubrey, B. J., Kelly, G. L., Janic, A., Herold, M. J. & Strasser, A. How does p53 induce apoptosis and how does this relate to p53-mediated tumour suppression? *Cell Death Differ* **25**, 104–113 (2018).

55.	Harper, J. W., Adami, G. R., Wei, N., Keyomarsi, K. & Elledge', S. J. The p21 Cdk-Interacting Protein Cipl Is a Potent Inhibitor of Gl Cyclin-Dependent Kinases. *Cell* **75**, 805–816 (1993).

56.	Brugarolas, J. *et al.* Radiation-induced cell cycle arrest compromised by p21 deficiency. *Nature* **377**, 552–557 (1995).

57.	Pan, R. *et al.* Synthetic Lethality of Combined Bcl-2 Inhibition and p53 Activation in AML: Mechanisms and Superior Antileukemic Efficacy. *Cancer Cell* **32**, 748-760.e6 (2017).

58.	Hemann, M. T. & Lowe, S. W. The p53-Bcl-2 connection. *Cell Death Differ* **13**, 1256–1259 (2006).

59.	Morselli, E., Galluzzi, L. & Kroemer, G. Mechanisms of p53-mediated mitochondrial membrane permeabilization. *Cell Research 2008 18:7* **18**, 708–710 (2008).

60.	Chen, J. The Cell-Cycle Arrest and Apoptotic Functions of p53 in Tumor Initiation and Progression. *Cold Spring Harbor Perspective in Medicine* **6**, (2016).

61.	Kracikova, M., Akiri, G., George, A., Sachidanandam, R. & Aaronson, S. A. A threshold mechanism mediates p53 cell fate decision between growth arrest and apoptosis. *Cell Death Differ* **20**, 576–588 (2013).

62.	Bharat, A. & Mohanakumar, T. Immune responses to tissue-restricted nonmajor histocompatibility complex antigens in allograft rejection. *J Immunol Res* **2017**, (2017).

63.	Vaidya, H. J., Briones Leon, A. & Blackburn, C. C. FOXN1 in thymus organogenesis and development. *Eur J Immunol* **46**, 1826–1837 (2016).

64.	Gordon, J. *et al.* Specific expression of lacZ and cre recombinase in fetal thymic epithelial cells by multiplex gene targeting at the Foxn1 locus. *BMC Dev Biol* **7**, (2007).

65.	Gordon, J., Bennett, A. R., Blackburn, C. C. & Manley, N. R. Gcm2 and Foxn1 mark early parathyroid- and thymus-specific domains in the developing third pharyngeal pouch. *Mech Dev* **103**, 141–143 (2001).

66. Sun, L. *et al.* Declining expression of a single epithelial cell-autonomous gene accelerates age-related thymic involution. *Aging Cell* **9**, 347–357 (2010).

67. O'Neill, K. E. *et al.* Foxn1 is dynamically regulated in thymic epithelial cells during embryogenesis and at the onset of thymic involution. *PLoS One* **11**, (2016).

68. Gui, J., Mustachio, L. M., Su, D.-M. & Craig, R. W. Thymus Size and Age-related Thymic Involution: Early Programming, Sexual Dimorphism, Progenitors and Stroma. *Aging Dis* **3**, 280–290 (2012).

69. van Ewijk, W., Shores, E. W. & Singer, A. Crosstalk in the mouse thymus. *Immunol Today* **15**, 214–217 (1994).

70. Petrie, H. T. Cell migration and the control of post-natal T-cell lymphopoiesis in the thymus. *Nat Rev Immunol* **3**, 859–866 (2003).

71. Alexandropoulos, K. & Danzl, N. M. Thymic epithelial cells: Antigen presenting cells that regulate T cell repertoire and tolerance development. *Immunol Res* **54**, 177–190 (2012).

72. Takaba, H. & Takayanagi, H. The Mechanisms of T Cell Selection in the Thymus. *Trends in Immunology* **38**, 805–816 (2017).

73. Takaba, H. *et al.* Fezf2 Orchestrates a Thymic Program of Self-Antigen Expression for Immune Tolerance. *Cell* **163**, 975–987 (2015).

74. Nishijima, H. *et al.* Aire Controls Heterogeneity of Medullary Thymic Epithelial Cells for the Expression of Self-Antigens. *The Journal of Immunology* **208**, 303–320 (2022).

75. Flanagan, S. P. 'Nude', a new hairless gene with pleiotropic effects in the mouse. *Genet Res* **8**, 295–309 (1966).

76. Nehls, M., Pfeifer, D., Schorpp, M., Hedrich, H. & Boehmt, T. New member of the winged-helix protein family disrupted in mouse and rat nude mutations. *Nature* **372**, 103–107 (1994).

77. Isotani, A., Yamagata, K., Okabe, M. & Ikawa, M. Generation of Hprt-disrupted rat through mouse←rat ES chimeras. *Sci Rep* **6**, 1–8 (2016).

78. Naito, Y., Hino, K., Bono, H. & Ui-Tei, K. CRISPRdirect: Software for designing CRISPR/Cas guide RNA with reduced off-target sites. *Bioinformatics* **31**, 1120–1123 (2015).

79. Mashiko, D. *et al.* Generation of mutant mice by pronuclear injection of circular plasmid expressing Cas9 and single guided RNA. *Scientific Reports* **3**, 1–6 (2013).

80. Heinz, N. *et al.* Retroviral and transposon-based Tet-regulated all-in-one vectors with reduced background expression and improved dynamic range. *Hum Gene Ther* **22**, 166–176 (2011).

81. Yusa, K., Zhou, L., Li, M. A., Bradley, A. & Craig, N. L. A hyperactive piggyBac transposase for mammalian applications. *Proc Natl Acad Sci U S A* **108**, 1531 (2011).

82. Tóth, E. *et al.* Cpf1 nucleases demonstrate robust activity to induce DNA modification by exploiting homology directed repair pathways in mammalian cells. *Biol Direct* **11**, 1–14 (2016).

83. Ho, Y., Wigglesworth, K., Eppig, J. J. & Schultz, R. M. Preimplantation development of mouse embryos in KSOM: Augmentation by amino acids and analysis of gene expression. *Mol Reprod Dev* **41**, 232–238 (1995).

84. Nikolova, T. *et al.* The γH2AX Assay for Genotoxic and Nongenotoxic Agents: Comparison of H2AX Phosphorylation with Cell Death Response. *Toxicological Sciences* **140**, 103–117 (2014).

85. Riss, T. L. *et al.* Cell Viability Assays - Assay Guidance Manual - NCBI Bookshelf. *Eli Lilly & Company and the National Center for Advancing Translational Sciences* https://www.ncbi.nlm.nih.gov/books/NBK144065/ (2004).

86. Tkatchenko, A. v. Whole-mount BrdU staining of proliferating cells by DNase treatment: Application to postnatal mammalian retina. *Biotechniques* **40**, 29–32 (2006).

87. Romano, R. *et al.* FOXN1: A master regulator gene of thymic epithelial development program. *Front Immunol* **4**, (2013).

88. Flanagan, S. P. 'Nude', a new hairless gene with pleiotropic effects in the mouse. *Genet. Res., Camb* **8**, 295–309 (1966).

89. Cowan, J. E., Takahama, Y., Bhandoola, A. & Ohigashi, I. Postnatal Involution and Counter-Involution of the Thymus. *Front Immunol* **11**, 897 (2020).

90. Zook, E. C. *et al.* Overexpression of Foxn1 attenuates age-associated thymic involution and prevents the expansion of peripheral CD4 memory T cells. *Blood* **118**, 5723–5731 (2011).

91. Luis, T. C. *et al.* Initial seeding of the embryonic thymus by immune-restricted lympho-myeloid progenitors. *Nat Immunol* **17**, 1424–1435 (2016).

92. Muro, R., Takayanagi, H. & Nitta, T. T cell receptor signaling for γδT cell development. *Inflamm Regen* **39**, (2019).

93. James, K. D., Jenkinson, W. E. & Anderson, G. T-cell egress from the thymus: Should I stay or should I go? *J Leukoc Biol* **104**, 275–284 (2018).

94. Stanislas, N. *et al.* Generation and Regeneration of Thymic Epithelial Cells. *Front Immunol* **11**, (2020).

95. Gao, Z., Herrera-Carrillo, E. & Berkhout, B. Delineation of the Exact Transcription Termination Signal for Type 3 Polymerase III. *Mol Ther Nucleic Acids* **10**, 36–44 (2018).

96. Kale, A. *et al.* Role of immune cells in the removal of deleterious senescent cells. *Immunity and Ageing* **17**, (2020).

97. Behmoaras, J. & Gil, J. Similarities and interplay between senescent cells and macrophages. *Journal of Cell Biology* **220**, (2021).

98. Poon, I. K. H., Lucas, C. D., Rossi, A. G. & Ravichandran, K. S. Apoptotic cell clearance: Basic biology and therapeutic potential. *Nat Rev Immunol* **14**, 166–180 (2014).

99. Elliott, M. R. & Ravichandran, K. S. The Dynamics of Apoptotic Cell Clearance. *Dev Cell* **38**, 147–160 (2016).

100. Kumari, R. & Jat, P. Mechanisms of Cellular Senescence: Cell Cycle Arrest and Senescence Associated Secretory Phenotype. *Front Cell Dev Biol* **9**, (2021).

101. Kumari, R. & Jat, P. Mechanisms of Cellular Senescence: Cell Cycle Arrest and Senescence Associated Secretory Phenotype. *Frontiers in Cell and Development Biology* **9**, (2021).

102. Fumagalli, M., Rossiello, F., Mondello, C. & D'Adda Di Fagagna, F. Stable cellular senescence is associated with persistent DDR activation. *PLoS One* **9**, (2014).

103. Petrova, N. v., Velichko, A. K., Razin, S. v. & Kantidze, O. L. Small molecule compounds that induce cellular senescence. *Aging Cell* **15**, 999–1017 (2016).

104. Kur-Piotrowska, A. *et al.* Neotenic phenomenon in gene expression in the skin of Foxn1-deficient (nude) mice - a projection for regenerative skin wound healing. *BMC Genomics* **18**, (2017).

105. Prowse, D. M. *et al.* Ectopic Expression of the nude Gene Induces Hyperproliferation and Defects in Differentiation: Implications for the Self-Renewal of Cutaneous Epithelia. *Dev Biol* 54–67 (1999).

106. Bukowska, J., Kopcewicz, M., Walendzik, K. & Gawronska-Kozak, B. Foxn1 in Skin Development, Homeostasis and Wound Healing. *Int J Mol Sci* **19**, 1956 (2018).

107. Militzer, K. & Militzer, K. Hair Growth Pattern in Nude Mice. *Cells Tissues Organs* **168**, 285–294 (2001).

108. Mecklenburg, L., Nakamura, M., Paus, R. & Sundberg, J. P. The nude mouse skin phenotype: The role of Foxn1 in hair follicle development and cycling. *Exp Mol Pathol* **71**, 171–178 (2001).

109. Ohigashi, I. *et al.* Aire-expressing thymic medullary epithelial cells originate from β5t-expressing progenitor cells. *Proc Natl Acad Sci U S A* **110**, 9885–9890 (2013).

110. Baik, S., Jenkinson, E. J., Lane, P. J. L., Anderson, G. & Jenkinson, W. E. Generation of both cortical and Aire(+) medullary thymic epithelial compartments from CD205(+) progenitors. *Eur J Immunol* **43**, 589–594 (2013).

111. Ribeiro, A. R., Rodrigues, P. M., Meireles, C., Santo, J. P. di & Alves, N. L. Thymocyte Selection Regulates the Homeostasis of IL-7–Expressing Thymic Cortical Epithelial Cells In Vivo. *The Journal of Immunology* **191**, 1200–1209 (2013).

112. Odaka, C. *et al.* Keratin 8 Is Required for the Maintenance of Architectural Structure in Thymus Epithelium. *PLoS One* **8**, (2013).

113. Nitta, T. & Takayanagi, H. Non-Epithelial Thymic Stromal Cells: Unsung Heroes in Thymus Organogenesis and T Cell Development. *Front Immunol* **11**, (2021).

114. James, K. D., Jenkinson, W. E. & Anderson, G. Non-Epithelial Stromal Cells in Thymus Development and Function. *Front Immunol* **12**, 232 (2021).

115. Gao, H. *et al.* The Lineage Differentiation and Dynamic Heterogeneity of Thymic Epithelial Cells During Thymus Organogenesis. *Front Immunol* **13**, (2022).

116. Nagaya, M. *et al.* Genetically engineered pigs manifesting pancreatic agenesis with severe diabetes. *BMJ Open Diabetes Res Care* **8**, e001792 (2020).

117. Mallet, V. O. *et al.* Conditional cell ablation by tight control of caspase-3 dimerization in transgenic mice. *Nature Biotechnology 2002 20:12* **20**, 1234–1239 (2002).

118. Pajvani, U. B. *et al.* Fat apoptosis through targeted activation of caspase 8: a new mouse model of inducible and reversible lipoatrophy. *Nature Medicine 2005 11:7* **11**, 797–803 (2005).

119. Wang, Z. v. *et al.* PANIC-ATTAC: A Mouse Model for Inducible and Reversible β-Cell Ablation. *Diabetes* **57**, 2137–2148 (2008).